Advanced Tilted-Airframe Unmanned Aerial Vehicle Transition Flight Control and Cruise Performance Analysis

By

ZHIXIANG CHAO

THESIS

Submitted in partial satisfaction of the requirements for the degree of

MASTER OF SCIENCE

in

Mechanical and Aerospace Engineering

in the

OFFICE OF GRADUATE STUDIES

of the

UNIVERSITY OF CALIFORNIA

DAVIS

Approved:

_____

Stephen Robinson, Chair

_____

C.P. van Dam

_____

Christina Harvey

Committee in Charge

2023

CONTENTS

LIST OF FIGURES

LIST OF TABLES

ABSTRACT

Advanced Tilted-Airframe Unmanned Aerial Vehicle Transition Flight Control and Cruise Performance Analysis

This thesis presents a conceptual design for a tilted-airframe unmanned aerial vehicle (UAV) that aims to address the challenge of detecting infected citrus trees by Huanglongbing (HLB) using a remote air sampling method. The tilted-airframe UAV is capable of vertical take-off and landing (VTOL) which can vertically take off and land in an orchard between trees and deploy an extendable boom to collect an air sample for HLB disease detection. The tilted-airframe UAV design is based on a tri-copter airframe with three key modifications: tilted-airframe, a novel moment (yawing and rolling) governing system, and a fixed-wing. When the UAV operates in VTOL mode, the airframe of the UAV is pitched up 45 degrees from the horizontal direction. The tilted-airframe concept simplified the UAV's mechanism design, with all motors fixed relative to the airframe and the whole airframe tilting during the flight mode transition. Furthermore, the tilted-airframe UAV utilizes a butterfly flap system on each side of the wing to control attitude and allows for constant RPM with fixed-pitch propellers during both hovering and the transition to cruise mode. The addition of a fixed wing increases the flight endurance, range, and cruise performance compared with a conventional multi-copter UAV. However, the tilted-airframe with a fixed-wing bring potential challenge for a stable hovering under wind disturbance and the power efficiency is not as good as a conventional fixed-wing UAV. Overall, this thesis explores the development of a tilted-airframe UAV for air sampling and HLB detection in citrus trees, focusing on the transition from hover to cruise mode, flight motion prediction, data collection, comparison, and cruise performance estimation.

ACKNOWLEDGMENTS

The guidance and support of countless individuals have been instrumental in shaping my path, and it is impossible to imagine reaching this point without their contributions.

First and foremost, I would like to express my deepest gratitude to my advisor, Professor Stephen K. Robinson, for his guidance, support, and mentorship throughout the course of this thesis. He has consistently been available for discussions, offering valuable insights and patiently addressing my concerns and questions. Through his encouragement and support, he has helped me grow as a researcher and instilled in me the confidence to pursue my research interests. I am truly grateful for the opportunity to have worked under his supervision and to have benefited from his vast experience and wisdom.

I would like to express my sincere appreciation to Professor van Dam and Professor Harvey, who served as the review committee members for my thesis. Their valuable feedback and insightful suggestions played a crucial role in enhancing the quality of my work, and I am deeply grateful for their support.

I would like to extend my thanks to all the individuals in the UC Davis Center for Human/Robotics/Vehicle Integration and Performance lab. The lab's collaborative and inclusive environment has provided me with a supportive space to explore new ideas and learn from diverse perspectives.

And lastly, thank you to my family for their unending support and encouragement throughout the completion of my thesis. I dedicate this thesis to all my family members who have played a part in shaping my academic and personal growth. Thank you for being a part of this incredible journey.

Chapter 1
Introduction

California's agricultural industry is overshadowed despite its substantial contributions to the state's economic diversity. California's farmers produced approximately $51.1 billion worth of agricultural commodities in 2021, providing employment for about 500,000 people in agriculture and related industries, which represent roughly 2% of the state's total employment [1]. According to Babcock's journal, California citrus is a major contributing factor to the economic value of the agricultural sector which accounts for 2.3% of total crop acres in the state and generated 6.7% of total crop revenue in 2020 [2]. Citrus Huanglongbing (HLB), also known as the citrus greening disease, is a highly destructive disease that causes yellowing of the leaves and reduces the marketability of fruit production. As reported by the California Department of Food and Agriculture (CDFA), HLB is the most devastating citrus disease, affecting all citrus cultivars and causing substantial economic and environmental losses by shortening the life of trees and making the fruit and juice inedible [3]. Furthermore, there is currently no curative or chemical method to control HLB. Thus, comprehensive control measures for HLB focus largely on the prevention of infection by eradicating infected trees. The tilted-airframe unmanned aerial vehicle (UAV) research platform has been designed to provide the first-ever remote air sampling method for rapid disease detection in citrus tree orchards. The UAV air sampling method aims to lower the cost and time of citrus tree health diagnosis, which would be more expensive and time-consuming if conducted manually by workers in trucks.

1.1 Research Objective

The tilted-airframe UAV was first designed by Ilya Anishchenko, a former UC Davis Human/Robotics/Vehicle Integration and Performance Laboratory (HRVIP) member [4]. Figure 1.1 shows the conceptual design of the tilted-airframe UAV configuration by Anishchenko.

Figure 1.1: Tilted-airframe UAV platform [4]

This novel design was capable of vertical take-off and landing (VTOL) flight capability but the initial research provided limited information on the UAV transition behavior to level cruise flight. In this thesis, the transition flight performance is studied and the cruise performance estimation is updated for the rebuilt prototype. There are three main goals for this research:

1) conducting the actual forward transition flight test with the prototype tri-copter UAV
2) modeling the UAV flight performance during transition from vertical flight to forward cruise sustained by wing lift
3) validating and improving the flight performance models with performance data obtained during the flight tests

The first goal of this research is to study the aircraft's transition flight from hover to cruise mode. The aircraft hovers with the airframe pitched up by 45 degrees. The aircraft transition to forward flight sustained by the wing involves a slight increase of tail motor thrust to slowly pitch the airframe down to cruise mode. Meanwhile, the two front motors operate at constant revolution speed (RPM), which provide both lift and forward thrust, due to the 45-degree offset on the wing.

The second goal for this research is to mathematically model the hover to forward flight transition performance. The predicted flight performance includes the time-dependent acceleration, velocity, and position in both longitudinal and vertical directions as well as angular acceleration, velocity, and angle of attack (AOA). The numerical modeling approach provides insight into the expected tilted-airframe UAV forward transition flight behavior and helps guide design of the test flight and data collection. After the forward transition modeling, transition flight tests were conducted to collect flight log data. This effort involved designing and building a test UAV prototype with improved performance from the original design, tuning the flight controller, safely operating the flight test, and collecting the flight log data. The collected flight test data was then compared to the predicted flight behavior to further study the forward transition flight of the tilted-airframe UAV and to validate the predictive models.

Lastly, this research provides an updated estimation for tilted-airframe UAV cruise performance. As with any winged aircraft, the tilted-airframe UAV cruise performance varies with angle of attack and the power setting of the electric motors. The cruise performance analysis provides an estimation of cruise airspeed, thrust and power requirements, flight duration, and range as different cruising angles of attack. The plots resulting from this research are included in this research to give insight into cruise performance and help determine the preferred UAV cruise angle of attack.

Chapter 2

Background

2.1 UAV Development and Platforms

The idea of using a machine that can fly remotely without a human on board has always been in many researchers' and engineers' minds. The idea of the unmanned aerial vehicle (UAV) brings many potential advantages such as reduced human risk, high maneuverability limit, and lower cost. Similar to a lot of technological advancements, UAVs are the result of the development carried out during military conflicts [5]. Figure 2.1 shows the Kettering Bug, one of the earliest experimental unmanned aerial torpedoes and it's first flight was on October 2, 1918. It was capable of striking ground targets up to 121 kilometers from its launch point with a cruise speed of 80 km/h. The Kettering Bug used a system of pre-set internal pneumatic and electrical controls to stabilize the aircraft [6].

Figure 2.1: Kettering Bug [7]

The de Havilland DH-82B Queen Bee, shown in Figure 2.2, was the first full production, full-sized, reusable, pilotless aircraft developed for anti-aircraft gunnery training [8]. According to O'Malley, it used a rotary dial control panel to operate pneumatic servos for controlling the aircraft's rudder, elevator, and throttle. The Queen Bee represented a major step forward in remote-control technology and also revealed shortfalls in the skills and efficacy of Royal Navy anti-aircraft.

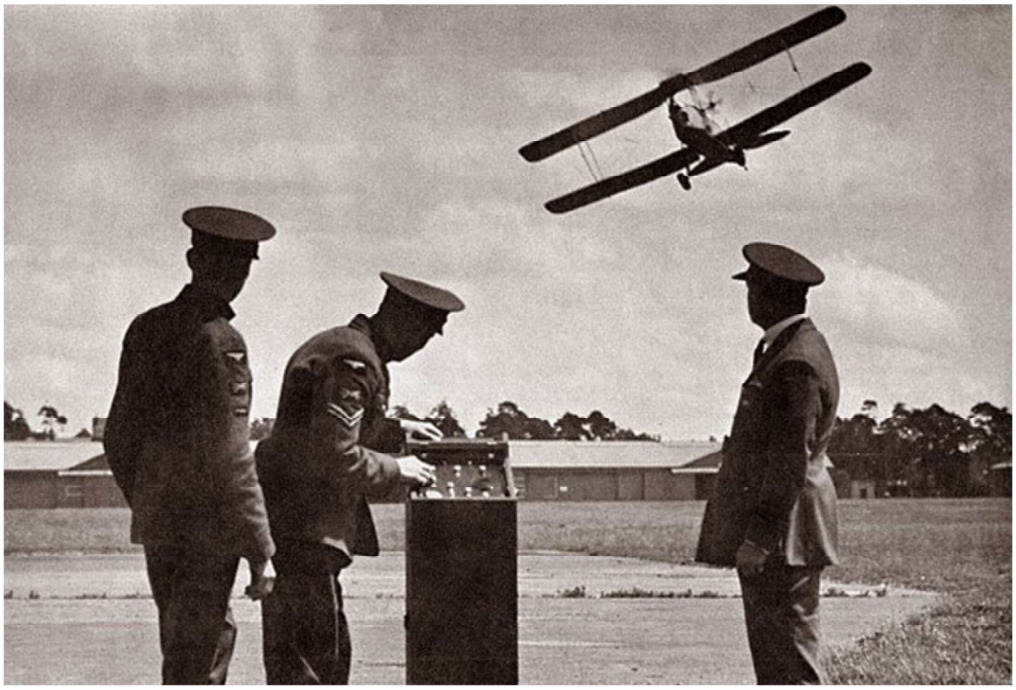

Figure 2.2: Queen Bee DH-82B [8]

In recent years, the miniaturization of electronics and the boost of computational power has allowed more compact flight control and navigation systems. Subsequently, this improved technology has made smaller size and low-cost UAVs possible. As Tsouros points out, the use of Internet of Things (IoT) devices like UAV in smart farming and precision agriculture can provide real-time environmental data, leading to faster decision-making and reduced costs [9]. Moreover, UAVs are a quickly evolving technology, and the use of unmanned aerial vehicle low-altitude UAV remote sensing (UAV-LARS) in precision agriculture is currently an area of great research interest and development [10,11].

A significant reduction in cost and an increase in yield are expected to result as technology evolves, which are expected to revolutionize agriculture by enabling decision-making in days instead of weeks [12]. The following subsections introduce the common UAV platforms and the tilted-airframe UAV platform in this research.

2.1.1 Fixed-wing UAVs

The fixed-wing UAVs are traditional aircraft where the majority of lift is generated by the fixed-wing. Fixed-wing UAV achieve forward motion through thrust generated by its onboard engines. It generates lift by utilizing the designed wing shape and the relative airspeed. During cruise aircraft are in an equilibrium state, where the thrust is equal to drag, and the lift is equal to the weight of the aircraft. The lift-to-drag ratio is used to compare the aerodynamic efficiency. The higher lift-to-drag ratio means better aerodynamic efficiency which brings advantages in flight time and range. Additionally, fixed-wing UAV typically has higher maximum flight speeds than multirotor, which makes it better suited for applications such as aerial mapping, surveillance, and monitoring. However, fixed-wing UAVs have their disadvantages. Depending on the UAV's cruise speed and weight, it may need a launch and recovery system or a runway for takeoff and landing, which needs special equipment and skills. In addition, fixed-wing UAVs are not capable of hovering in a stationary position and required a minimum flight velocity, known as the stall velocity, to maintain altitude. The control surfaces redistribute the airflow to control the roll, pitch, and yaw movement of the UAV which does not offer the same level of maneuverability as a multirotor.

2.1.2 Multirotor

The multirotor is a rotorcraft that uses multiple rotors to fly. A multirotor is classified according to its number of rotors. For example, a multirotor with four rotors is named a quadrotor. In general, there is an even number of rotors to counter the rotational torque while operating such as in quadcopters and hexacopters. In other words, for each clockwise rotating rotor, there is a counterclockwise rotor. But there are some special cases in which the number of rotors is an odd number. For example, the helicopter has a single main rotor and an antitorque device such as the tail rotor or fantail. The tilted-airframe UAV considered in this research is classified as a tri-copter. Figure 2.3 shows a Y-shape tri-copter, two rotors spin in opposite directions, but the remaining rotor generates torque that attempts to spin the tri-copter in the opposite direction. To counteract this effect, a rear servo is employed to tilt the rear rotor and compensate for the torque, similar to how a helicopter's tail rotor functions.

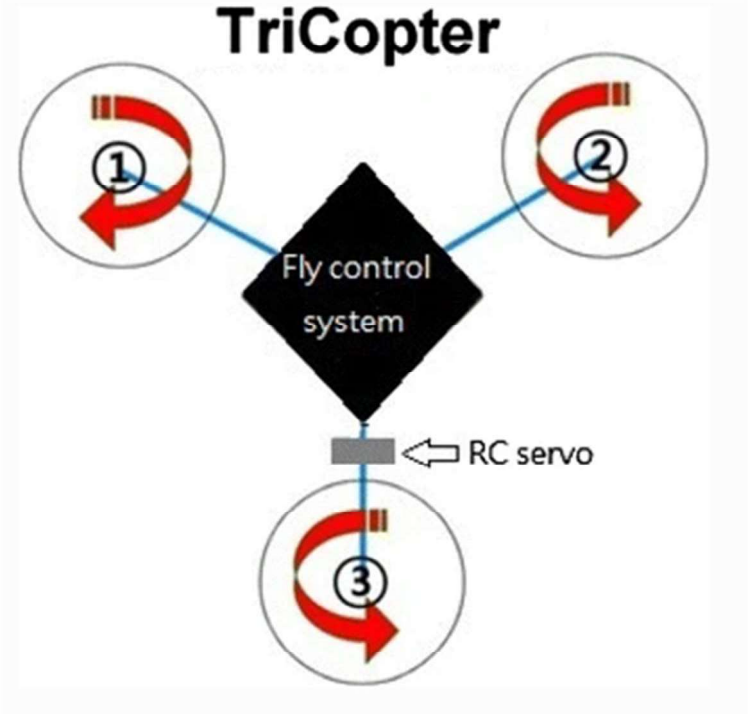

Figure 2.3: Typical Y-shape tri-copter model [13]

A quadcopter is designed with four rotors placed at equal distances from the center of gravity. Quadcopters are also popular among hobbyists due to their ease of use and the ability to perform aerial stunts and acrobatics. Figure 2.4 shows the flight control of the quadcopter:

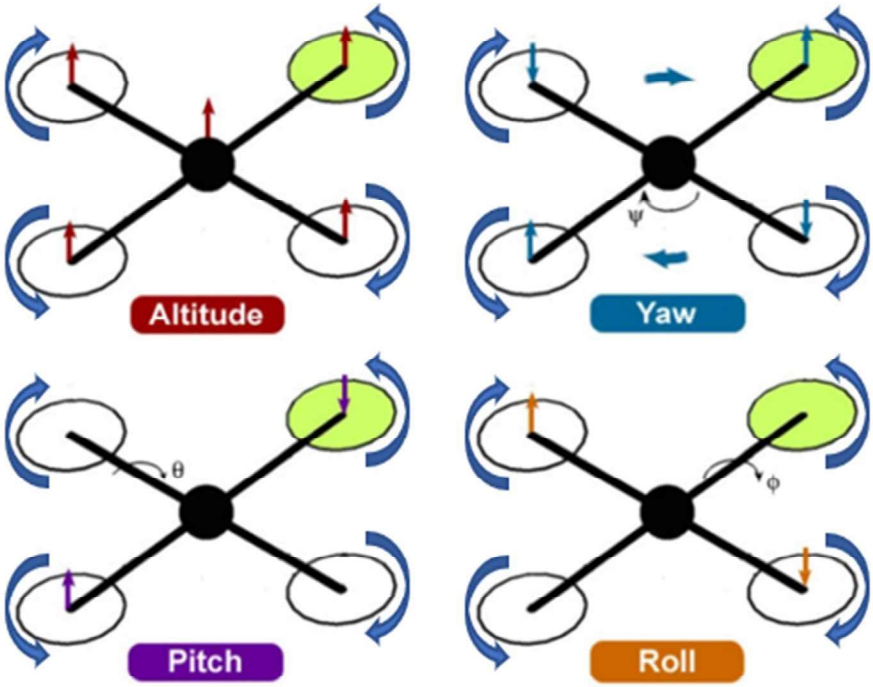

Figure 2.4: Quadcopter flight control diagram [14]

The arrows in the flight control diagram indicate the change in rotor speed for quadcopter flight control. The rotors diagonally oriented are rotating in the same direction. The lift is generated only by the rotor thrust which enables the multirotor to hover stationary if needed. All rotors increase the rotational speed to gain altitude. Yawing motion is controlled by lowering the rotors speed in one diagonal and increasing the rotors speed in another diagonal. Pitch motion is controlled by speeding up one rotor and speeding up the diagonal rotor. Roll motion is similar to the pitch motion by varying the speed of the rotor pair along a different axis. After several years of operation development, the multirotor flight controller is well developed making it easier to fly compared to a fixed-wing UAV.

In addition, the multirotor is capable of vertical take-off and landing which is runway independent. Quadcopters are now widely used for recreation, research, and industry due to their beginner-friendly nature, VTOL capability, and maneuverability. However, there are also several disadvantages to consider, such as shorter flight time and lower forward flight speed compared to a fixed-wing UAV [15]. When all of the lifting force is generated by electric motor-driven propellors, all segments of flight are a significant drain on the stored power in the onboard battery. These limits on flight time and range restrict the uses of the multirotor for short-flight missions only. Fixed wings efficiently generate lift without moving parts, requiring only forward thrust. An optimal UAV for orchard air sampling might take advantage of both multi-copter vertical take-off and landing, plus the cruise efficiency of a fixed wing. This is the motivation for the current UAV design and accompanying performance research.

2.1.3 VTOL Fixed-wing Aircraft

There have been many attempts to combine the advantages of fixed-wing UAVs (long endurance and range) with the advantages of the multirotor (VTOL and stational hover capability) [16]. The current UC Davis/HRVIP VTOL fixed-wing aircraft is a hybrid of fixed-wing and multirotor which brings the advantages of both types of UAVs. The VTOL fixed-wing aircraft can operate as a multirotor during take-off and landing without a paved runway; it can then transition to cruise like a fixed-wing aircraft, using the wing to generate lift. Considering pervious hybrid UAV and aircraft designs, the most common VTOL fixed-wing aircraft are tiltrotor and standard VTOL. The tiltrotor UAV (shown in Figure 2.5) has propulsion system that can tilt relative to the airframe to different angles to transition between hover and cruise flight. During take-off and landing, the tiltrotor engines are perpendicular to the airframe like a multirotor.

Figure 2.5: Bell Eagle Eye tiltrotor aircraft [17]

For aircraft like this, the tilt-rotors pitch forward during the hover-to-cruise transition to pick up relative airspeed. The wing starts generating lift as the UAV speeds up. During cruise, wing lift generates the majority of the lift instead of the propeller forces. The reduction in propeller forces results in reduced power consumption when cruising. The tilt-rotors reverse the tilting motion, i.e., pitch rearward, during landing. Ideally, the tiltrotor VTOL UAV cruise-like fixed-wing aircraft increases cruise efficiency compared to a multicopter. However, the complex motor-tilt mechanism adds significant extra weight which reduces the payload capacity and increases the power consumption during VTOL. Furthermore, the complex motor-tilt mechanism and aerodynamics during transition add a potential failure mode.

As opposed to tiltrotor VTOL aircraft, standard VTOL aircraft do not have a motor tilting mechanism, all motors are fixed in position relative to the airframe. Instead, the standard VTOL has two sets of propulsion systems, one provides lifting force perpendicular to the airframe when hovering and another provides propulsion parallel to the airframe when cruising. Figure 2.6 is an example of a typical non-tilting VTOL aircraft that includes a fixed wing for cruise lift.

Figure 2.6: JOUAV standard VTOL aircraft [18]

The standard VTOL/rigid wing takes off like a multirotor, and transitions to cruise by using the propulsion engine to gain relative airspeed. A specially designed flight controller allows stable flight at every point of the transition phase between VTOL and fixed-wing mode. The engines that are perpendicular to the airframe shut down once the aircraft gains enough airspeed to support its weight with wing lift. During cruising flight, a standard VTOL employs the motor aligned parallel to the airframe to provide thrust. The standard VTOL does not have complex tilt mechanisms compared to the tiltrotor VTOL. However, the two sets of propulsion systems also add extra weight and complexity.

To sum up, the added wing generally makes a hybrid VTOL fixed-wing UAV more efficient in generating lift than a multirotor. The design trade-offs necessary to achieve vertical takeoff and landing capability often result in added weight and complexity, which can limit the VTOL fixed-wing aircraft's range and endurance compared to a pure fixed-wing design. Therefore, the flight distance and endurance of a VTOL fixed-wing should surpass the multirotor but fall short of the fixed-wing aircraft. In addition, there is no need for a runway during take-off and landing. Therefore, there are missions that a VTOL fixed-wing aircraft can complete that multirotor and fixed-wing aircraft cannot. The tilted-airframe UAV is another example of a VTOL fixed-wing aircraft, and further details on this concept are provided in Section 2.2.

2.2 UC Davis Tilted-Airframe UAV

The UC Davis tilted-airframe UAV is a unique design that features an airframe tilted 45 degrees with respect to the ground when hovering or landing. The rotors are fixed at another 45 degrees angle with respect to the airframe, so 90 degrees from the ground during hovering. This novel design means that there is no need for a rotor-tilting mechanism because the UAV transitions between rotor-hover mode and wing-cruise mode by simply tilting the entire airframe. Figure 2.7 shows the CAD model of the UC Davis tilted-airframe UAV :

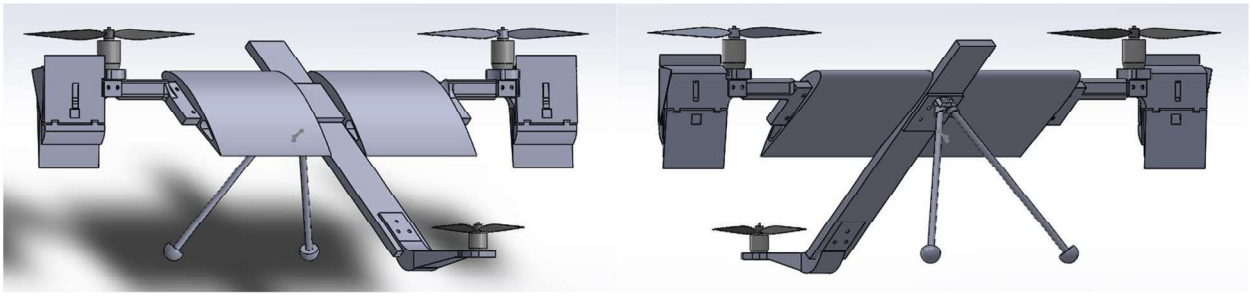

Figure 2.7: CAD drawing of tilted-airframe UAV

Figure 2.8 includes the side view of the tilted-airframe UAV operates in hover and cruise mode.

Hover flight mode Cruise flight mode

Figure 2.8: Tilted-airframe UAV different flight modes

2.2.1 Aircraft Configuration

The UC Davis tilted-airframe UAV keeps the rotors oriented perpendicular to the ground when hovering. This configuration makes the tilted-airframe UAV capable of VTOL. The tail rotor is a variable-speed propeller that controls the tilting/pitching of the UAV. This approach does not require a change of angle between the airframe and rotors. This design eliminates the need for the complex rotor tilting mechanism as a tiltrotor UAV. Furthermore, the tilted-airframe UAV with a fixed rotor position reduces the weight and the chance of tilting mechanical failures compared to the tiltrotor UAV.

Unlike the conventional quadcopter, standard tri-copters control vehicle roll by varying the rotor speed on either wing and control yaw with a servo motor or rudder at the tail. The butterfly flap system, shown in Figure 2.9, is a unique moment governing system used in the UC Davis tilted-airframe UAV. It effectively controls airframe roll and yaw while keeping the rotors at a constant RPM, which is different from the conventional quadcopter and standard tri-copters.

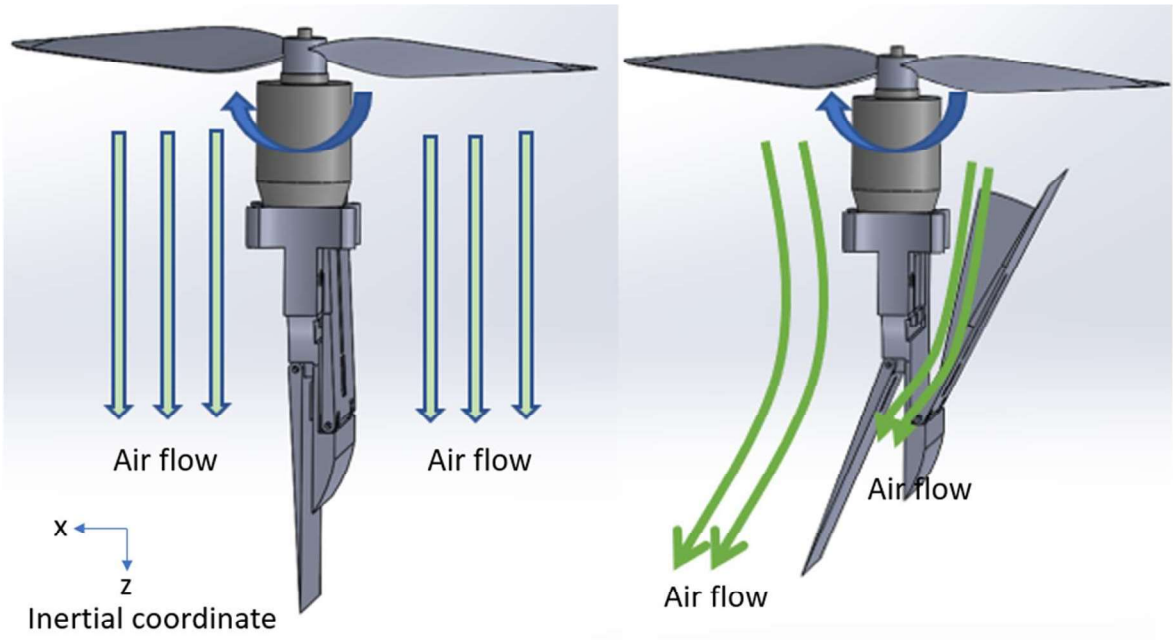

Figure 2.9: Butterfly flap system retracted (left) and deployed (right)

Each butterfly flap system consists of two flaps: the front flap is oriented tailing-edge down and the back flap is oriented tailing-edge up. And the deployment and retraction of each flap can be done independently. The aircraft yawing and rolling control forces are generated by deflecting the airflow. Figure 2.10 shows the forces acting on the flaps when the flaps are deployed.

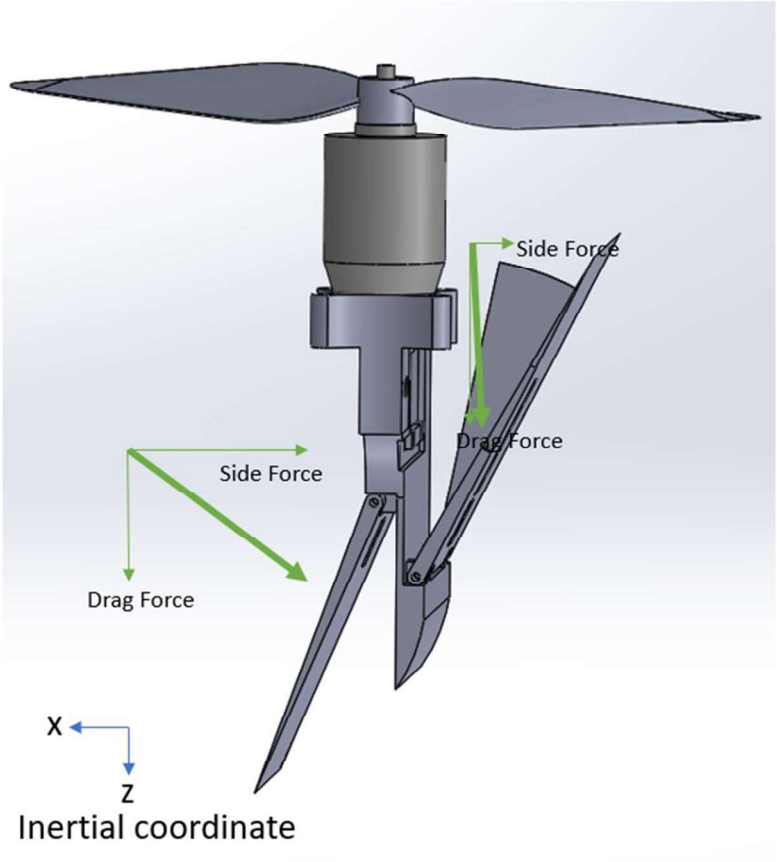

Figure 2.10: Force applied on flaps

The reaction force applied to each flap has two force components: drag and side force. The side force contributes to the UAV's yawing moment, while the drag force contributes to the UAV's rolling moment. Based on the magnitude of these force components, the front flap is used to control the vehicle's yaw, which eliminates the need for a yawing servo motor at the tail. The back flap is used to control the UAV's roll.

The design of the butterfly flaps for roll and yaw control allows the two front rotors to operate at the same constant speed and does not require rapid rotor speed change for UAV roll and yaw control. While it is possible to achieve a rapid change in rotor speed with current rotors, this becomes more challenging when dealing with much larger rotors due to the significantly higher amount of angular momentum required to effect such changes. This research will thus investigate and verify this new moment control system concept which may have the potential to be used for large-scale UAVs.

The third critical feature of the tilted-airframe UAV is the specially selected airfoil shape that is chosen to provide wing lift during the transition from hover to cruise flight and back. With the high angle of attack (45 degrees) during hovering and the low angle of attack during cruising, the forward transition starts from an angle of attack past wing stall and is reduced until the flow reattaches. This, when selecting the airfoil shape, the low angle of attack lift performance and the post-stall lift characteristics of the wing were both significant design drivers.

2.2.2 Mission Concept

The tilted-airframe UAV platform is designed to support citrus orchard agriculture, specifically for rapid air sampling for HLB disease. The typical mission profile is illustrated in Figure 2.11.

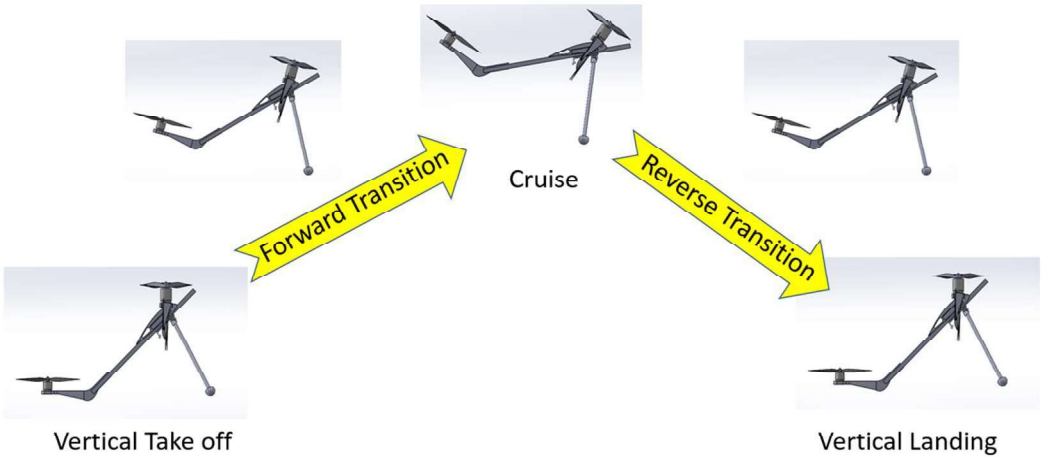

Figure 2.11: Typical mission profile

On a typical orchard air-sampling mission, the concept of operations is as follows:

The UAV performs a vertical take-off from the operation base. Then it performs a forward transition from hover to cruise by slightly increasing the tail rotor speed to pitch down the airframe. When the forward transition is complete, the wing will generate a lift sufficient to allow the UAV to operate at lower rotor speed (lower power consumption) and cruise toward the targeted citrus orchard. When the UAV approaches the landing site between trees, a reverse transition starts by pitching the airframe up. When the reverse transition is complete, the UAV enters hover mode. The UAV performs final loitering and landing within proximity to the tree and turns off the motors. The UAV equipped with an extendable boom will deploy the boom near the leaves of a citrus tree to collect an air sample. After the sample has been collected, the boom will retract and the UAV will repeat its flight mission, retrieving the air sample for analysis to detect HLB disease.

To summarize, the tilted-airframe UAV requires VTOL capability, cruise efficiency, and loitering stability. The tilted-airframe and rotors enable the VTOL capability. The selected airfoil shape helps the tilted-airframe transition and cruise efficiency. The butterfly flap system and tail motor control the roll, yaw, and pitch motion, thereby providing control of the tilted-airframe UAV in vertical takeoff and landing, hover, and cruise.

Chapter 3
Design and Build

The tilted-airframe UAV built during this research adapts and modifies an earlier design by former UC Davis HRVIP Lab graduate student Ilya Anishchenko [4]. The original (and patent pending) tilted-airframe and butterfly flap concepts are unchanged. However, the wing size, airfoil shape, overall dimensions, and control system have all been adjusted to fully enable the transition behavior. In addition, this study considered a relatively smaller size UAV compared to Anishchenko's prototype to safely test the transition behavior. Minor changes and justifications for motors, propellers, and butterfly flaps system were made during the flight test process as will be discussed. The newly built tilted-airframe UAV is shown in Figure 3.1.

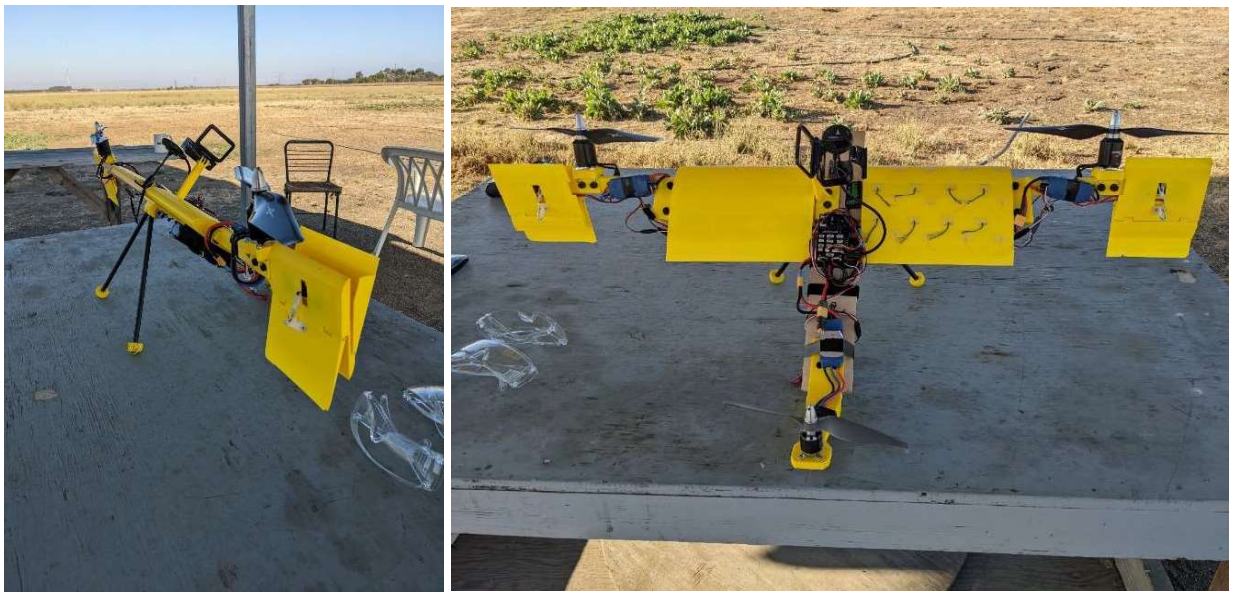

Figure 3.1: Tilted-airframe UAV prototype

3.1 Preliminary Sizing

Each component of the tilted-airframe UAV's mass and position relative to an airframe-anchored origin at the nose of the UAV is provided in Table 3.1. The total take-off mass of the UAV is calculated by summing up all the masses. The body-fixed axis system is used as a reference frame for measurements or calculations (Figure 3.2).

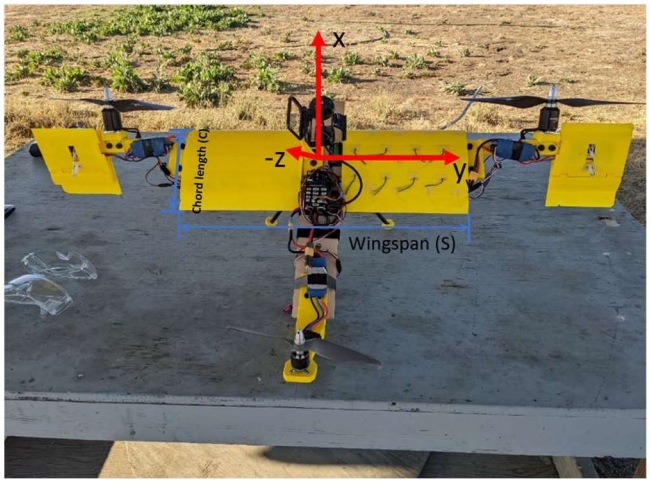

Figure 3.2: UAV reference frame

Table 3.1: Mass breakdown table

	mass (g)	count	x(cm)	mx(g*cm)	I_{yy}(g*cm^2)
Wing flap joint	44	2	12	1056	52
3D printed wing	103	2	15	2987	204
Butterfly flap+motor+ESC	461	2	11	10142	2017
Wing spar	206	1	11	2348	590
Fuselage	155	1	23	3550	14911
Battery	561	1	23	12903	55073
Tail structure	83	1	48	3984	101142
Tail ESC	92	1	39	3588	61753
Tail motor	82	1	57	4674	158089
GoPro	176	1	11	2006	504
Controller	70	1	24	1680	8329
GPS module	32	1	8	256	830
Landing gear	72	1	23	1649	6926
Sum	2745			50823	410420

*Note: 1) mx (Moment of each component about the aircraft nose)
2) I_{yy} (Pitch moment of inertia)
3) ESC (Electronic speed controller)

An estimated center of mass and pitch moment of inertia of a tilted-airframe UAV can be calculated using the following equations:

$$x_{cm} = \frac{\sum_{i=1}^{N} m_i x_i}{\sum_{i=1}^{N} m_i} \quad \text{(eq 3.1)}$$

$$I_p = \sum_{i=1}^{N} m_i r_i^2 \quad \text{(eq 3.2)}$$

x_{cm} center of the mass

m_i component mass

x_i component relative position to the aircraft nose

I_p pitch moment of inertia

r_i relative position from x_{cm}

The tilted-airframe UAV wing has an effective wingspan of 56 cm and a chord length of 18 cm. The aspect ratio and Reynolds number are important values to consider when selecting the airfoil shape of the wing. The equation of the aspect ratio of the rectangular wing is:

$$AR = \frac{s}{c} \quad \text{(eq 3.3)}$$

AR aspect ratio

s wingspan

c chord length

Since the UAV cruise speed has been determined through testing to be approximately 15 m/s, the estimated Reynolds number can be calculated as:

$$Re = \frac{\rho u L}{\mu} \quad \text{(eq 3.4)}$$

Re Reynolds number

ρ air density

u vehicle velocity

L reference length (wing chord c)

μ dynamic viscosity of the fluid

The resulting aspect ratio and Reynolds number are 3.11 and 1.8×10^5, respectively.

3.2 Hardware Selection

The hardware choices for the experimental UAV are described in the following subsections.

3.2.1 Airframe

Basswood was selected for the UAV's fuselage and wing spars. Basswood is a low-density material and easy to craft while being much stronger than cardboard or balsa. This choice was important because the early outdoor test flights for transition were expected to possibly involve uncontrollable impacts. Therefore, it was necessary to choose a more rigid structure to reduce the potential damage. The current prototype has a total wingspan of 116 cm and a fuselage length of 46 cm while Anishchenko's UAV prototype had a total wingspan of 112 cm and a fuselage length of 141 cm. Reducing the fuselage length resulted in increased aerodynamic efficiency and smaller aircraft size, which in turn reduced the weight of the aircraft.

3.2.2 Airfoil Selection

As mentioned in the aircraft configuration section, the airfoil shape needed to be specifically selected based on the tilted-airframe flight requirement. At the beginning of the forward transition, the flow is initially separated from the wing surface because of the high (45 deg) AOA. Then, as the airframe pitches down, the flow starts to reattach to the wing surface. When selecting the airfoil shape, both the pre-stall and post-stall characteristics of the wing were considered.

For the transition study, it was found that a relatively high post-stall lift coefficient helps the UAV gain lift early during the forward transition. And a smooth (rather than abrupt) stall characteristic helps the steady forward transition during the flow reattachment as the airspeed increases and the angle of attack decreases.

Normally, the lift and drag coefficient is available for the angle of attack less than 30 degrees. There are two ways to obtain the lift and drag coefficient for the larger angle of attack range. The first method is to use the XFOIL software tool to simulate the post-stall region, but as an inviscid method, XFOIL has poor accuracy for post-stall analysis [19]. The second method is to use available wind tunnel test data. The current research uses the wind tunnel test data published by the pre-NASA National Advisory Committee for Aeronautics for NACA 44xx series airfoil sections [20]. The test data covers the angle of attack from -10 to 110 degrees which provides enough data for the forward transition analysis.

Based on C. Ostowari and D. Naik's trend study, when increasing the thickness ratio (t/c), the lift coefficient increases, and the drag coefficient decreases [20]. In addition, the higher thickness ratio shows a smoother stall which is preferred for tilted-airframe transition, since the vehicle transitions through wing stall twice on every flight. Therefore, the airfoil with a higher thickness ratio is preferred as it increases the lift coefficient, reduces the drag coefficient, and performs a smooth post-stall recovery. Wind tunnel test data for NACA 44xx series is available for a thickness ratio range from 9% to 18%. Therefore, the highest thickness ratio airfoil (18%) NACA 4418 was selected for the tilted-airframe UAV.

Wind tunnel test data by Ostowari and Naik includes Reynolds number range from 2.5×10^5 to 1.0×10^6 with an increment of 2.5×10^5 [20]. The estimated Reynolds number for the tilted-airframe UAV is about 1.8×10^5, so the wind tunnel data with a Reynolds number 2.5×10^5 were selected as the closest comparable data. Figures 3.3-3.5 show the wind tunnel test data for NACA 4418 wing section:

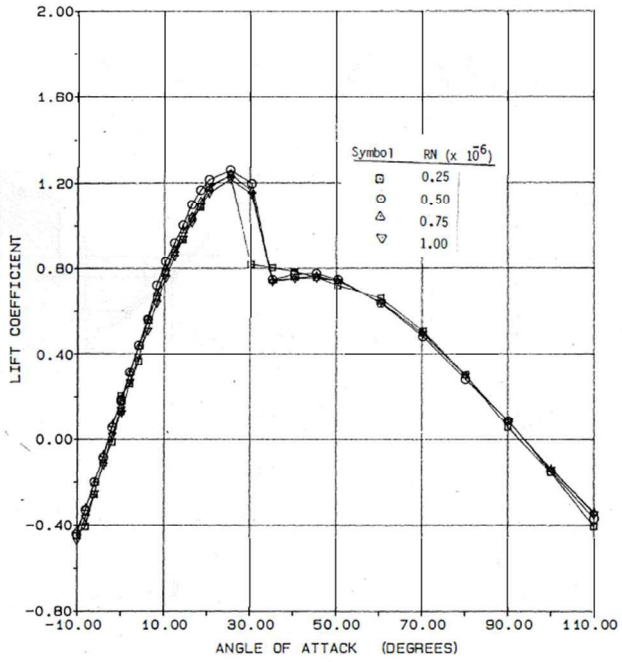

Figure 3.3: Lift curve for NACA 4418 with AR=6 [20]

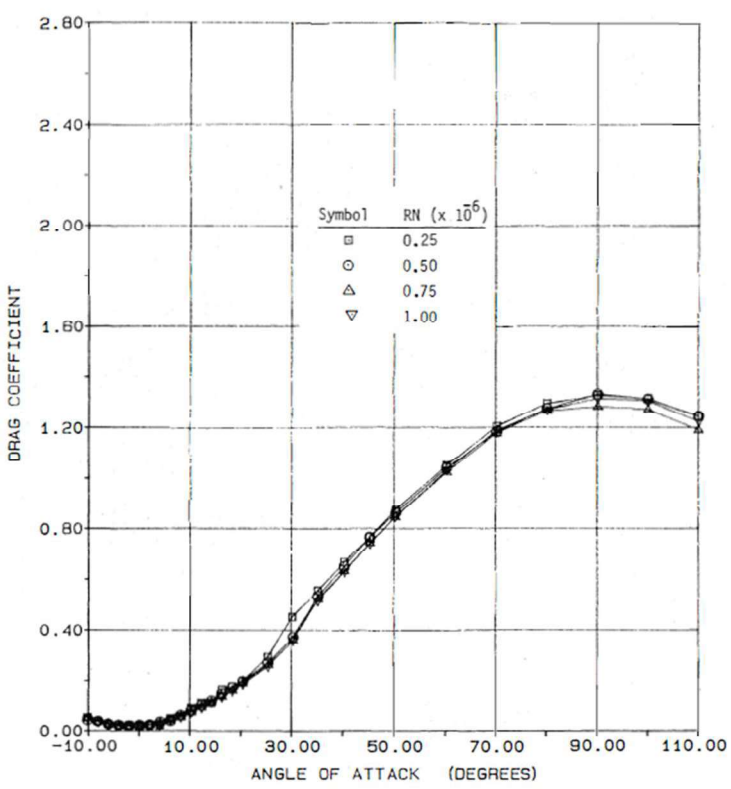

Figure 3.4: Drag curve for NACA 4418 with AR=6 [20]

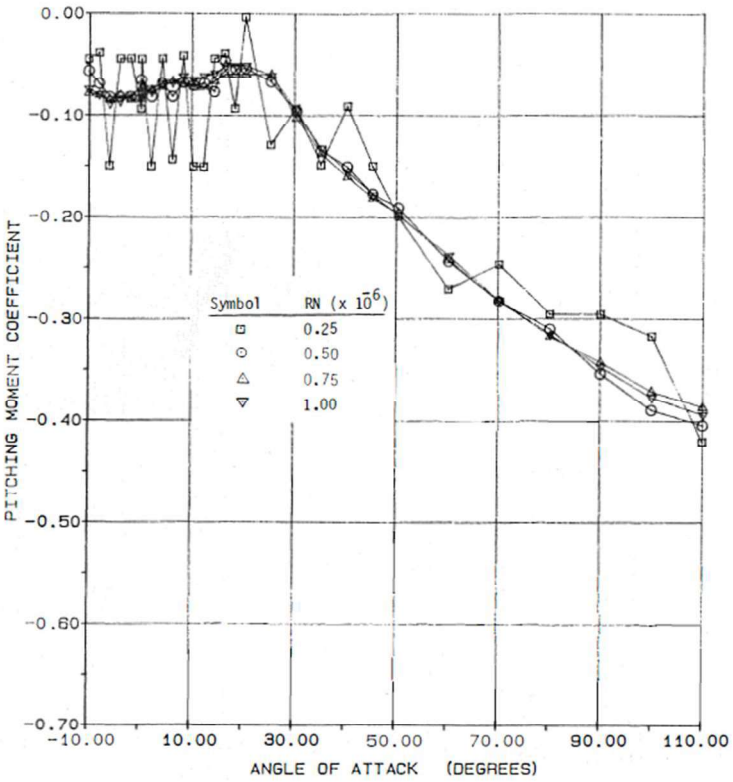

Figure 3.5: Pitching moment coefficient for NACA 4418 with AR=6 [20]

3.2.3 Motor and Propeller Selection

The motors and propellers are selected based on Anishchenko's propeller thrust and power trend study [4]. The large-diameter, low-pitch propellers generate more thrust at the same input power than the small-diameter high-pitch propellers [4]. Moreover, as thrust requirements increase, the slope of the thrust vs power curve decreases, indicating that the propeller/motor system becomes less efficient. It is beneficial to run the motor at the lowest power settings possible to minimize the energy drawn from the battery. Because the front motors are located much closer to the center of gravity than the tail motor, they have a much shorter moment arm, resulting in the majority of the hovering thrust being provided by the front motors. The tail motor is mainly used for pitch control. The thrust required by each motor is calculated (eq. 5.1 and 5.2) using the total take-off weight and relative position of each motor from the center of gravity (moment arm).

Based on the trend study, the front motors have larger operating power compared to the tail motor, therefore the size of the front motors should be larger than the tail motor. The 35-48 brushless DC motor is selected for the front motors and the 28-30 brushless DC motor is selected for the tail motor. The first number indicates the motor diameter and the second number indicates the motor height. For example, a 35-48 DC motor is 35 mm in diameter and 48 mm in height. The propeller sizing follows the same reasoning, the larger motor is usually paired with a larger size propeller. The front propeller size is 13 × 4.5 and the tail propeller size is 10 × 4.5. The first number represents the radius of the propeller in centimeters, while the second number represents the propeller pitch, which is the distance the propeller would move forward in one full rotation through a soft solid in centimeters.

Figure 3.6 is the power versus thrust curve for the front and tail motor and propeller set. Figure 3.6 verified the trend study that it is more efficient to run the motor at a relatively lower power setting. The power required for a 28-30 DC motor is higher than a 35-48 DC motor when providing the same amount of thrust.

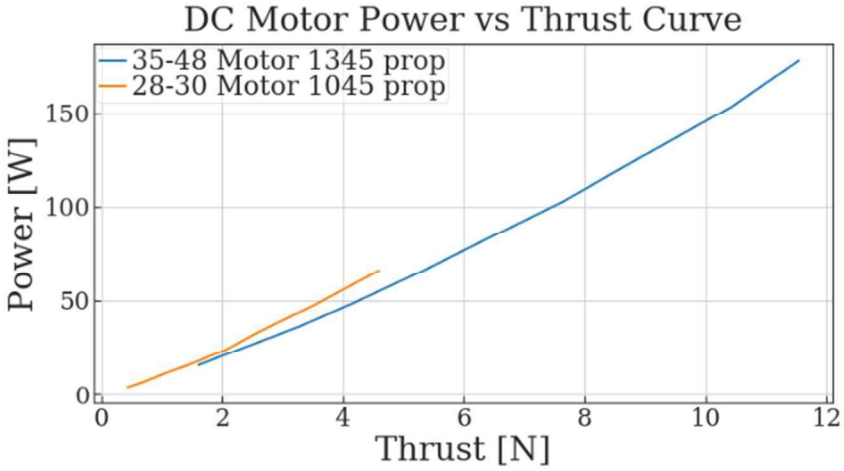

Figure 3.6: Motor power versus thrust curve

3.2.4 Flap Modification

During the test flight, it was experimentally observed through manual flight control that the inverted flap of the butterfly flap system may not be providing enough drag force for the effective roll moment control of the UAV. The reason is that the butterfly flap system has two flaps; the front flap has a high dynamic pressure, and the reverse flap has a low dynamic pressure. Figure 3.7 illustrates the motor's rotating direction and the dynamic pressure on each flap:

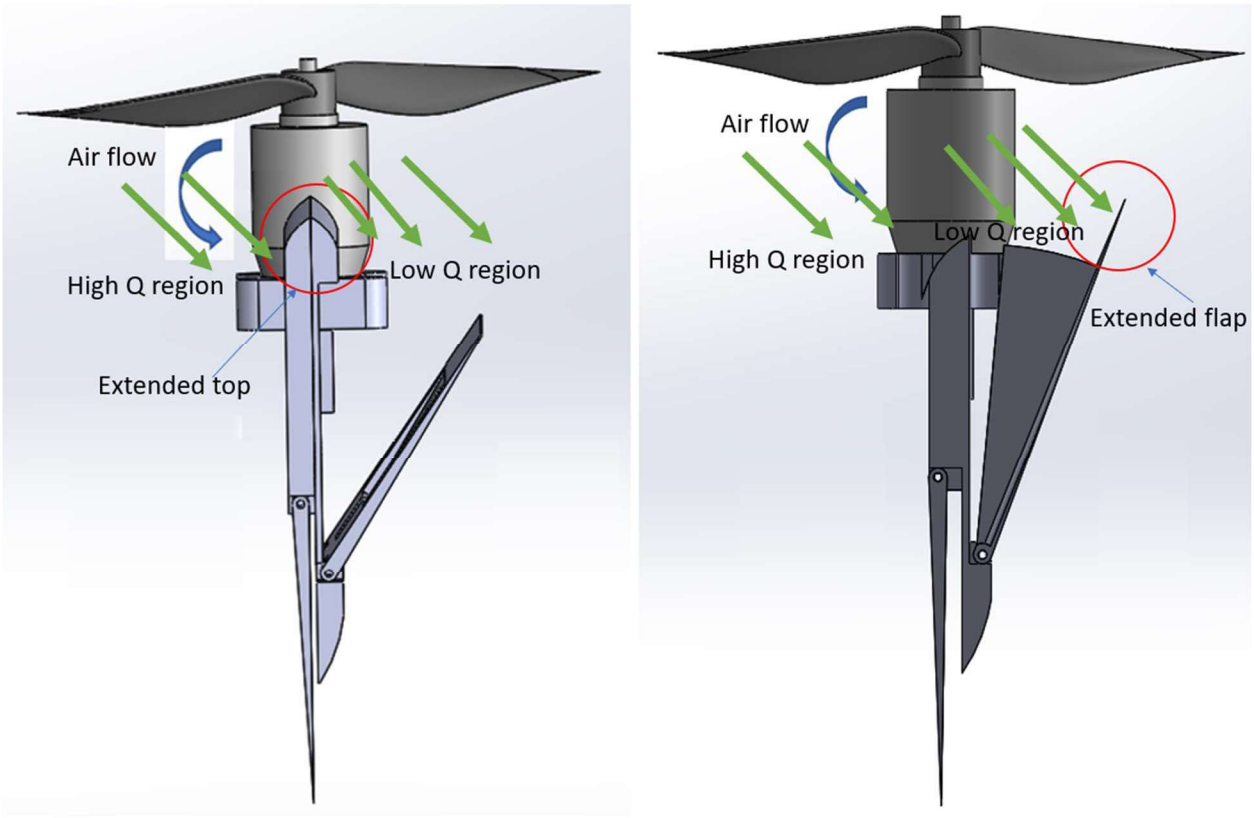

Figure 3.7: Butterfly flap system original (left) and modified (right)

The original design has an extended top that blocks a significant amount of airflow. Additionally, the short reverse flap cannot control much of the airflow when the deployment angle is small. The modified design shortens the flap holder top and extends the reverse flap that allows more airflow on the reserve flap which enhances the capability of thrust control.

Additionally, the modified design adds a thin fin on the side to prevent air leakage. This results in deceleration of the air flow speed, thereby increasing the drag force for roll moment control of the UAV. The difference is noticeable when the flap is deployed at a small angle (less than 10 degrees). Measurement of changes in drag forces on the inverted flap versus flap deployment angle shows significant improvement in roll moment control. Figure 3.8 shows the comparison of the two designs:

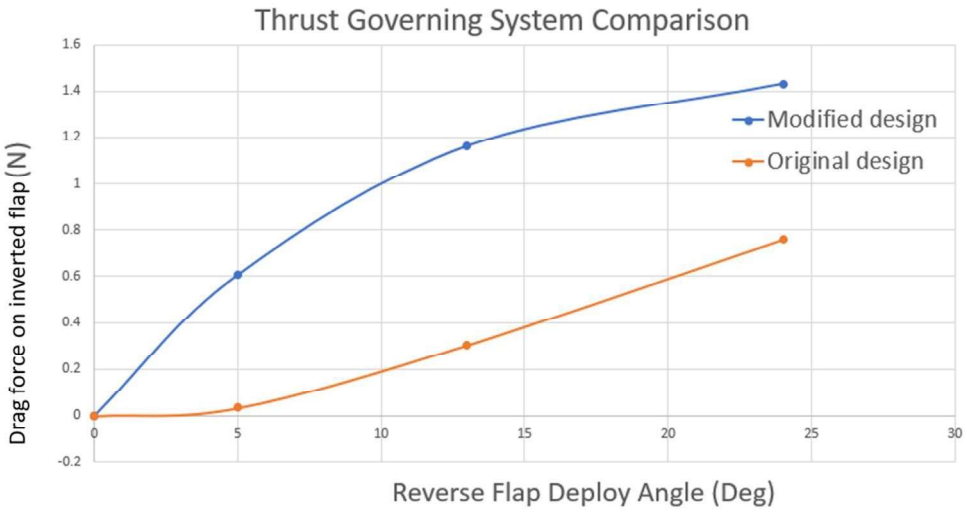

Figure 3.8: Drag force on inverted flap comparison

The modified flap system has an overall higher force control capability than the original design. Specifically, when the flap deployment angle is small, the original design barely provides any control for the thrust. That causes a noticeable time delay and possible overshot for UAV attitude control. The resulting plot (Figure 3.8) shows significant improvement in drag force on the inverted flap for the modified moment control system.

3.3 Summary of UAV Parameters

The tilted-airframe UAV characteristic parameters are summarized in Table 3.2:

Table 3.2: Tilted-airframe UAV characteristic parameters

Parameters	**Values**	**Units**
Total mass	2745	g
Center of gravity in body x-axis (Measure from the nose of the fuselage)	18.5	cm
Pitching moment of inertia	410420	$g*cm^2$
Front motors moment arm	6	cm
Tail motor moment arm	32.7	cm
Battery pack	4S Lipo 7000mAh	
Wingspan (total)	116	cm
Fuselage length	46	cm
Wingspan (effective)	56	cm
Wing area	1008	cm^2
Reynolds number	2×10^5	
Airfoil shape	NACA 4418	
Wing chord length	18	cm
Aspect ratio (AR)	3.11	
Front motors	3548 900KV	
Tail motor	2830 1000KV	
Front propellers	13 × 4.5	
Tail propeller	10 × 4.5	
Servo motors	MG90S	

Parameters in Table 3.2 are later used for numerical analysis of the transition flight performance.

Chapter 4
Control and Tuning

The flight controller is the key system of a UAV. Similar to Anishchenko's research, the Pixhawk controller board was selected [4]. The Pixhawk series controller is a widely used hardware package for academic and commercial UAVs with a fast central processing unit (CPU) speed and the ability to customize the airframe setting. A newer version Pixhawk 4 controller board was used for this research. The Pixhawk 4 controller is an advanced autopilot designed and made in collaboration with Holybro and the PX4 team. The Pixhawk 4 controller was connected to a Global Positioning System (GPS) module, remote receiver (RC), and power management board (PM07) with pulse-width modulation (PWM) signals. The GPS module and the inertia measurement unit (IMU) provide the detailed UAV state and sensor data which can later use for UAV tuning and flight performance analysis. The RC receiver captures wireless signals from the RC transmitter and processes the commands from the ground pilot. The power management board power the flight controller, motors, and servos. Furthermore, the power management board uses the PWM signal output from the controller to produce the desired control for DC motors and servo motors for UAV attitude and stability control. The tilted-airframe UAV in this research has three brushless DC motors and four servo motors. The electronic speed controllers (ESCs) use the main PWM signals output to control the rotation direction and speed of the brushless DC motors.

While the servo motors use the auxiliary PWM signal output to control the butterfly flap system. A wiring diagram for the power management board is included in Figure 4.1.

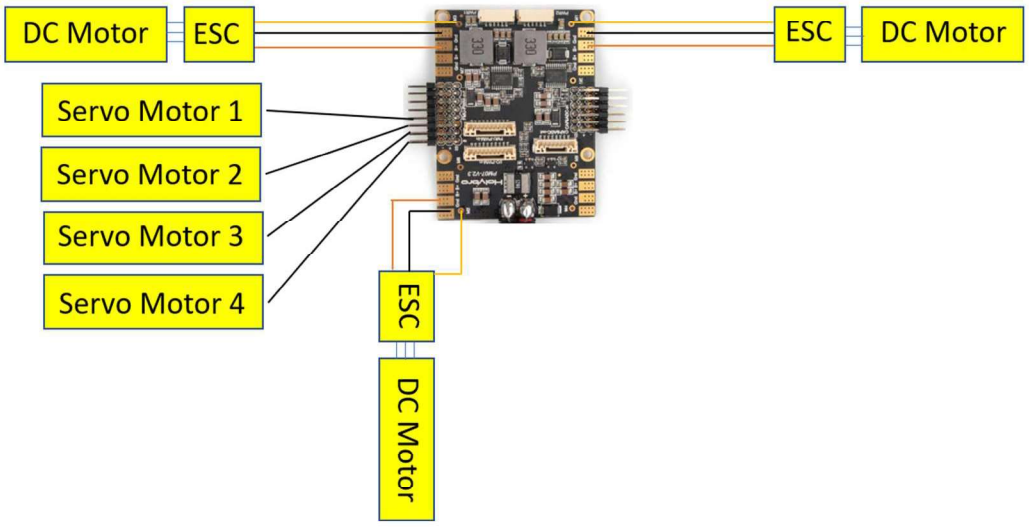

Figure 4.1: Wiring diagram for the power management board

4.1 Control Architecture

The controller architecture is based on a proportional (P), integral (I), and derivative (D) (PID) controller. Figure 4.2 shows sample rate controller architecture.

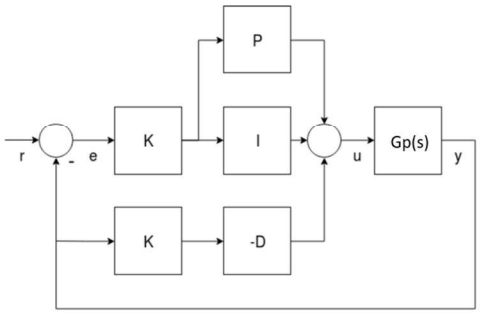

Figure 4.2: Rate controller architecture

The gyroscope measures the body's angular rate, *y*. Then the difference between the rate setpoint r and the measured rate y is the error *e*. A total gain K multiplies the error term and feeds the value to the PID gain. The values after proportional, integral, and derivative gain add up as the PID controller output *u*.

The governing equation of the standard PID controller is:

$$G(s) = K_p + sK_d + \frac{K_i}{s} \quad \text{(eq 4.1)}$$

K_p proportional gain

K_d derivative gain

K_i integral gain

The Gp(s) is a system transfer function that relates the controller output and the aircraft's dynamic response.

4.2 Mixer and Actuator

The system transfer function mentioned in Section 4.1 is called the mixer. The role of the mixer is to take the PID output commands and translate them to the actuator commands which give the control signal for corresponding motors and servos [21]. There are two types of mixers used for the tilted-airframe UAV which are main and auxiliary mixers. The main mixer file is used for the brushless DC motor control while the auxiliary mixer file is used for the servo motor control. The sample mixer setting has parameters as shown below:

S: <group> <index> <-ve scale> <+ve scale> <offset> <lower limit> <upper limit>

A control group can be used for attitude control, core flight controls, or payload gimbal control. An output group refers to a physical bus such as the initial 8 PWM outputs for servos. Both control and output groups have a maximum of 8 normalized (-1..+1) command ports, which can be configured and adjusted through the mixer. Essentially, the mixer determines the connection between the 8 control signals and 8 outputs. The second term index indicates the aircraft's motion controlled by the corresponding actuator such as roll, pitch, yaw, and throttle. The scale term scales the PID output and changes the sign of the output if necessary. For example, when rolling is commanded, one side of the inverted flap will open while the other remains closed.

The scale term will set the correct sign for the inverted flap to open and scale zero for the other inverted flap to remain closed. The fifth term sets an offset to the zero position. An offset command only applies if the flap is not fully closed at the rest position. The lower and upper limit parameters set the minimum and maximum range of the actuator response.

The following procedures set up the mixer values to convert the PID output signal to the actuator control signal. First, all motors and servos should be unloaded before setting up the mixer values for safety concerns. The summing mixer order should agree with the actuator signal pin connection order. Based on the types of actuators, motors, or servo, the mixers should be stored in the correct mixer file types. The control group number should be consistent for all the mixers set up. The group number is 0 for the transition flight behavior study. The index is set to the expected aircraft dynamic response. Figure 4.3 listed the index number for aircraft dynamic response for control group #0.

Figure 4.3: Index number for aircraft dynamic control [21]

For example, for the tail motor used for pitch control, the index number should be 1. For the scales and limits, the values are multiplied by a factor of 10000 and range from -10000 to 10000. The main motor throttle control is a special case in which the throttle ranges from 0 to 20000 with -10000 offset. To test out the actuator behavior, send the remote signal for each control and verify the expected actuator behavior. If the actuator tends to behave opposite to the control command, then the sign of the scale parameters needs to switch.

4.3 Tuning

Five degrees of freedom (DOF) test roller was used for the hovering test and tuning. The UAV was mounted to a plate with a free rotating joint that provided the necessary degrees of freedom for roll, pitch, and yaw. A supporting rod connecting to the roller provides the test freedom for the aircraft's up and down motion. Last, the roller plate provides the freedom to move sideways. Figure 4.4 shows the 5 degrees of freedom test rig:

Figure 4.4: 5 DOF test rig

There are two objectives while tuning the aircraft's hovering dynamics. First, testing and tuning of the aircraft were performed for a self-controlled stable hovering condition. The second step involves evaluating the ability of the aircraft to follow commands and recover for a stable flight.

Aircraft tuning mainly focuses on rate tuning because it has the largest contribution to the aircraft's dynamic behavior. Parameters used for rate control are P, I, D, K, and the maximum rate. The proportional gain P is used to minimize the tracking error. A low P value will cause the aircraft to react slowly, and a high P value will cause high-frequency oscillations.

The integral gain I keeps a memory of the error. The low I gain will keep an offset between the desired and the actual rate over a long time while the high I gain will cause slow oscillations. The derivative gain D is used for rate damping. Besides, the noise term will be amplified by derivative gain. An overshoot after a step input indicates a low D gain and a twitchy behavior indicates a high D gain. The overall gain K is similar to the proportional gain P but K gain serves as a multiplier for all the gain parameters (P, I, and D). The maximum rate parameters determine the maximum rotation rate around three axes which contributes to the actuator response speed.

The following steps are the general procedure that was used for rate tuning. First, the P and D gains were decreased until the aircraft is capable of take-off. Then, the aircraft's response to a step input when hovering was observed. If the reaction to the step input was minimal, the P gain should increase slightly. If the reaction oscillates, the D and I gain should be adjusted based on the oscillation types. If a high overshoot occurs after tuning the PID parameters, then lowering the maximum rate (thus lowering the actuator response speed) solves the problem. If the aircraft's dynamic response was hard to observe, the flight log data can provide a better reference for fine-tuning. An ideal tuning expects the rate estimated to follow the rate setpoint closely with minimum lagging, overshoot, and oscillation. Figures 4.5 and 4.6 demonstrate the pitch response of a tilted-airframe UAV during flight testing, with one representing a poor response and the other showing a satisfactory response.

Figure 4.5: Example of poor pitch angle dynamic response

Figure 4.6: Example of satisfactory pitch angle dynamic response

In Figure 4.5, the pitch angle of the aircraft is seen to oscillate frequently, indicating a poor response to commands and a failure to follow the pitch setpoint. In contrast, Figure 4.6 depicts the pitch angle following the setpoint closely, with a maximum difference of less than 2 degrees.

Chapter 5
Transition Flight Modeling

Chapter 5 covers the numerical approach for transition flight modeling including the assumptions that were made during flight modeling, as well as the modeling methodology and the results.

5.1 Assumptions

First, the numerical analysis includes only the wing contribution to the aircraft's total lift and drag analysis. Initially, the drag due to other components is not taken into account. The flap system and the fuselage contribute to the total aircraft lift and drag, which leads to an underestimation of the total drag. The experiment of an improved total drag measurement carried out during this study is presented in Section 5.3. Second, the reference 3D wing data is obtained under the test conditions: Reynolds number of 0.25 million and an aspect ratio of 6. However, the true aspect ratio for the tested aircraft is 3.11. In general, the lower wing aspect ratio results in lower wing efficiency. The lift generated by the wing is overestimated when performing the numerical analysis. Solving for the cruise velocity using the aerodynamic data set at 0.25 million Reynolds number yields a corresponding value of 20 m/s. However, this value exceeds the targeted cruise velocity for the aircraft. But, based on the reference 3D wing data, the effect of the Reynolds number is not significant. The reference data for the pitching moment coefficient is unsuitable for numerical analysis due to its irregular pattern. Therefore, the wing pitching moment is not considered during numerical analysis, and the net pitching moment is determined by only considering the thrust of the motors.

This results in an underestimation of the net pitching down moment for the forward transition. The pitch angle represents the angle between the horizontal and the UAV body x-axis, while the angle of attack indicates the angle between the freestream velocity vector and the UAV body x-axis. It's important to acknowledge that these angles may not always be identical since the freestream velocity vector may not necessarily be horizontal. Therefore, assuming that the angle of attack is equal to the pitch angle, as done in numerical estimation, may introduce errors in the calculation of the angle of attack.

5.2 Methodology

The numerical analysis first calculates the thrust of each motor based on the take-off weight of the aircraft, the center of gravity, and the location of the motors. The equations are:

$$T_f = \frac{r_2}{r_1+r_2} W \quad \text{(eq 5.1)}$$

$$T_r = \frac{r_1}{r_1+r_2} W \quad \text{(eq 5.2)}$$

T_f Front motors thrust

T_f Tail motor thrust

W Weight of the aircraft

r_1 Front motor moment arm

r_2 Tail motor moment arm

A small percent change of tail motor thrust is selected to initiate a non-zero net pitching moment. The pitching acceleration is estimated using the non-zero pitching moment and the aircraft's pitching moment of inertia. The equation is:

$$\dot{\omega} = \frac{M}{Ip} \quad \text{(eq 5.3)}$$

$\dot{\omega}$ Angular acceleration

M Pitching moment

Then, the angular velocity and the angle of attack for the following time step are estimated using the first order of Talyor expansion:

$$\omega_{i+1} = \omega_i + \dot{\omega} dt \quad \text{(eq 5.4)}$$

$$\alpha_{i+1} = \alpha_i + \omega_i dt \quad \text{(eq 5.5)}$$

ω Angular velocity

α Angle of attack

dt Time step size

The next step is to estimate the lift and the drag of the aircraft from the angle of attack and the horizontal velocity. The equations for the lift and drag are:

$$L = \frac{1}{2}\rho v^2 C_L S \quad \text{(eq 5.6)}$$

$$D = \frac{1}{2}\rho v^2 C_D S \quad \text{(eq 5.7)}$$

L Lift

D Drag

ρ Air density

v Horizontal speed

C_L Lift coefficient

C_D Drag coefficient

S Reference wing area

The net vertical force is a combination of the vertical thrust component of all motors and the wing lift. Similarly, the net horizontal force is a combination of the horizontal thrust components from all of the motors and the drag force.

$$L_{net} = L_{gen} + L - W \quad \text{(eq 5.8)}$$

$$T_{net} = T_{gen} - D \quad \text{(eq 5.9)}$$

L_{net} Net vertical force

L_{gen} Vertical force component by motors

T_{net} Net horizontal force

T_{gen} Horizontal force component by motors

The estimation of the vertical and horizontal force components from the motors involves the use of trigonometry and is dependent on the pitch angles. This method assumes that the motor thrust remains constant throughout the estimation process. Once the net vertical and horizontal force is estimated and the mass of the aircraft is known, the relative acceleration, velocity, and displacement can be calculated using a similar method as angular motion estimation. The time step size is the same as used for angular motion estimation.

The vertical and horizontal motion estimation equations are:

$$a_h = \frac{T_{net}}{m} \quad \text{(eq 5.10)}$$

$$v_{h_{i+1}} = v_{h_i} + a_h dt \quad \text{(eq 5.11)}$$

$$h_{i+1} = h_i + v_{h_i} dt \quad \text{(eq 5.12)}$$

$$a = \frac{T_{net}}{m} \quad \text{(eq 5.13)}$$

$$v_{i+1} = v_i + a dt \quad \text{(eq 5.14)}$$

$$d_{i+1} = d_i + v_i dt \quad \text{(eq 5.15)}$$

m	Mass of the aircraft
a_h , v_h, h	Vertical acceleration, speed, displacement
a, v, d	Horizontal acceleration, speed, displacement

At this point, a full cycle of the motion estimation for a given time step is performed. To finish the numerical analysis for full forward transition analysis, repeat Equation 5.4 to Equation 5.15. Figure 5.1 shows the flow chart for tilted-airframe UAV forward transition analysis. The legend indicates the input, outputs, and order to proceed with the flow chart. The flow chart uses the percent change of the tail motor thrust as the input. The outputs are the UAV's horizontal, vertical, and angular motion parameters.

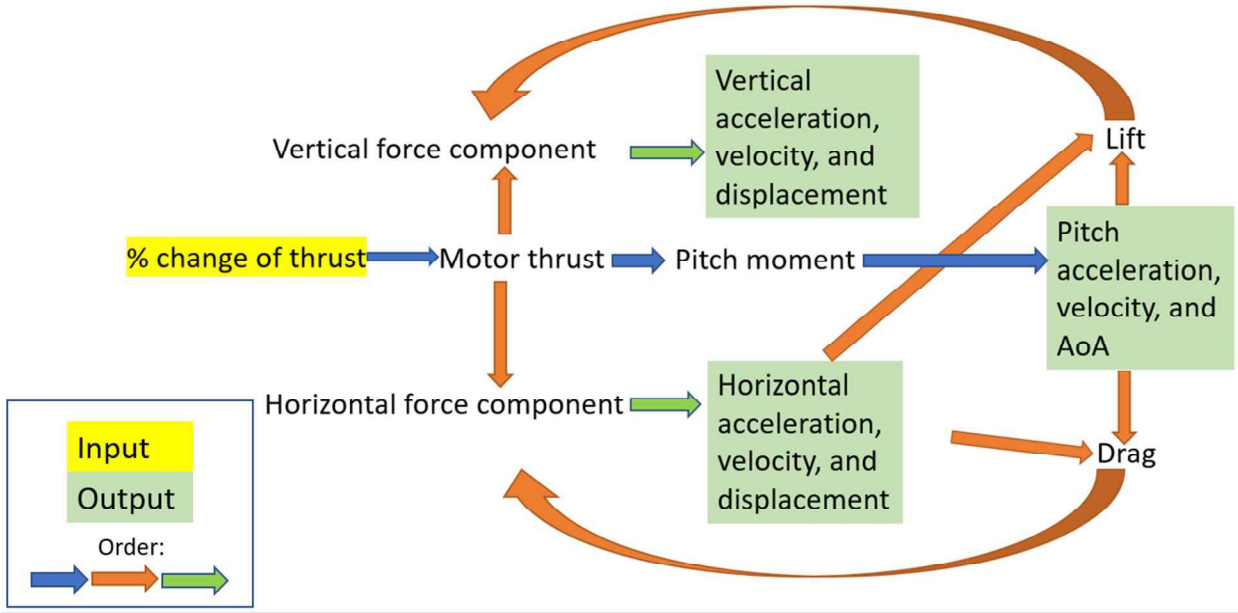

Figure 5.1: Numerical analysis flow chart

5.3 Improved drag estimation

To improve the model accuracy, the total drag coefficient measurement using a load cell was performed. The test was set up using the 5 DOF test rig mentioned in the previous section with some modifications. The standing rod is replaced by a 3D-printed structure that can adjust the UAV AOA for each test. Figure 5.2 illustrates the adjustable AOA fixture.

Figure 5.2: Adjustable AOA fixture

The test rig is fastened on a truck cargo bed and the truck is driving backward to minimize the flow interaction. The fishing line connects the load cell and the roller plate to measure the drag force as the pulling force. The tested angle of attack range from 0 to 45 degrees with 5 degrees increment for each trial. The data recorded included the acceleration and deceleration periods. Only the relative constant data are selected to indicate the truck is driving at a constant speed, there is no force component measurement caused by acceleration. The drag force is obtained by averaging the selected data for each angle of attack test. Based on the known truck speed, air density, and reference wing area, the coefficient of the whole UAV can be calculated by solving the drag equation (Equation 5.7). Figure 5.3 shows the test rig used for drag measurement.

Figure 5.3: The test rig for drag measurement

Figure 5.4 is the drag curve comparison:

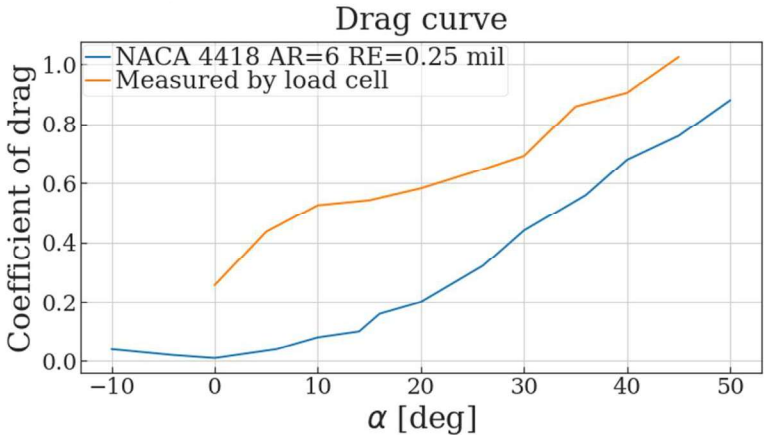

Figure 5.4: Wing and total UAV drag curve comparison

The results agree with the reasoning mentioned in the assumption section. The total drag of the UAV is much larger than the wing drag only. The improved results using the measured total drag of the UAV are included in forward transition flight modeling for comparison.

5.4 Numerical Analysis Results

The forward transition starts by slightly increasing the tail motor speed to give a nose-down pitching moment. Then all the motor speeds hold constant during the forward transition. The net moment is constant with the assumption that only motor thrusts contribute to the net moment (Section 5.1). Then, the expected estimation of angular speed is proportional to the first power of the time in the input variables, whereas the expected estimation of the tilt angle is proportional to the second power of the time in the input variables. Figure 5.5 is the change in the tilt angle during the transition which agrees with the expected trend. There was no noticeable difference between the two numerical results because the wing pitching moment is not taken into account based on the third assumption in Section 5.1.

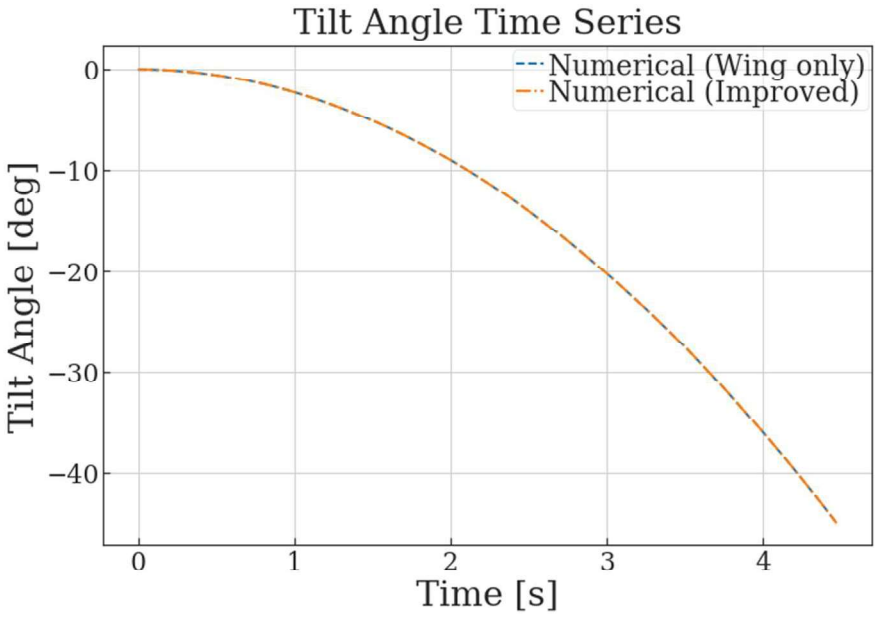

Figure 5.5: The tilt angle versus time (simulated)

The transition from 45 to 0 degrees tilt angle takes about 4.5 seconds. However, the transition should end before reaching the zero-degree tilt angle. The endpoint of the transition is determined when the total lift generated is equal to the aircraft weight. That means the aircraft reaches an instantaneous equilibrium state in the vertical direction.

Figure 5.6 and Figure 5.7 show the simulation results for vertical velocity and vertical displacement during the forward transition. The change of vertical velocity is less than 1 m/s while the change of the vertical displacement is less than 3 m. These indicate the change in vertical velocity and altitude for a slow transition process (change of 0.24% tail motor thrust) is small and appropriate for the future flight test. The difference in vertical velocity and displacement result using different drag curves is barely noticeable. Especially, during the end of the forward transition, the difference starts occurring. The red line indicates zero change in vertical speed which means the vertical acceleration is equal to zero. The UAV reaches an instantaneous lift and weight equilibrium at this moment. This might consider the endpoint for forward transition, and the mode switches to cruise mode at this time. The estimated forward transition time is about 3.3 seconds.

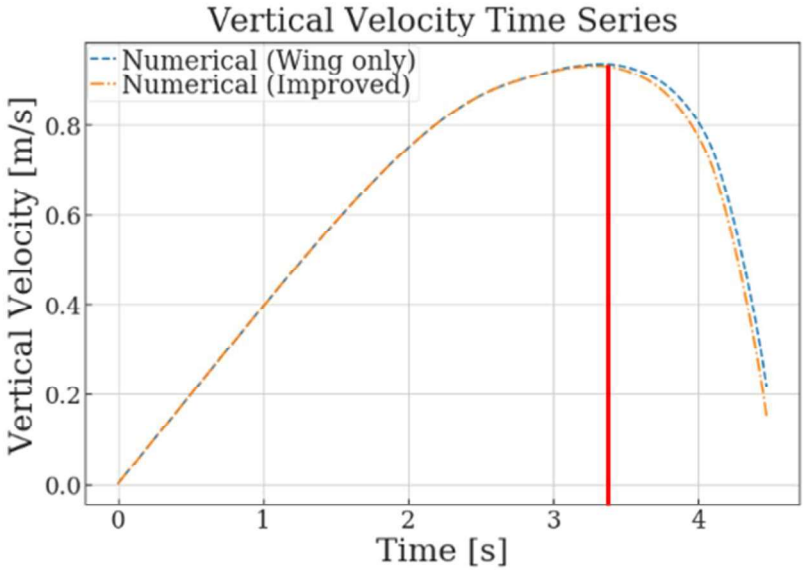

Figure 5.6: The vertical velocity versus time (simulated, vertical equilibrium point marked)

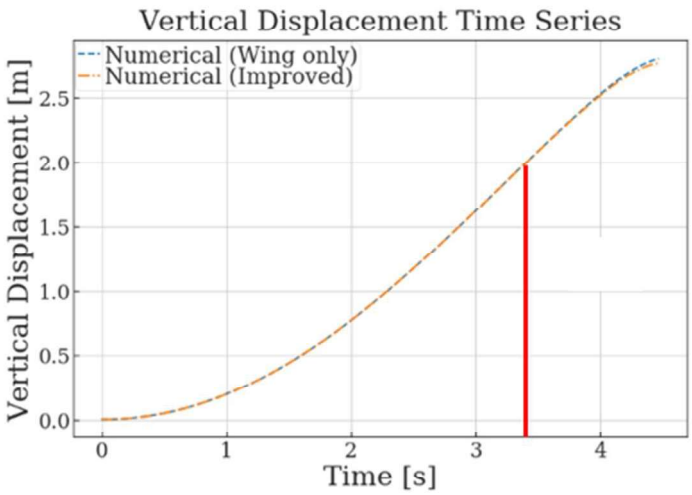

Figure 5.7: The vertical displacement versus time (simulated, vertical equilibrium point marked)

Similarly for horizontal velocity and displacement, Figures 5.8 and 5.9 indicate the maximum values for horizontal velocity and displacement. For the forward airframe tilting from 45 degrees to 0 degrees AOA, the maximum change of horizontal velocity is less than 11 m/s while the maximum change of horizontal displacement is less than 12 m. The expected horizontal velocity and displacement are approximately 5 m/s and 4 m, respectively, once the UAV reaches instantaneous lift and weight equilibrium.

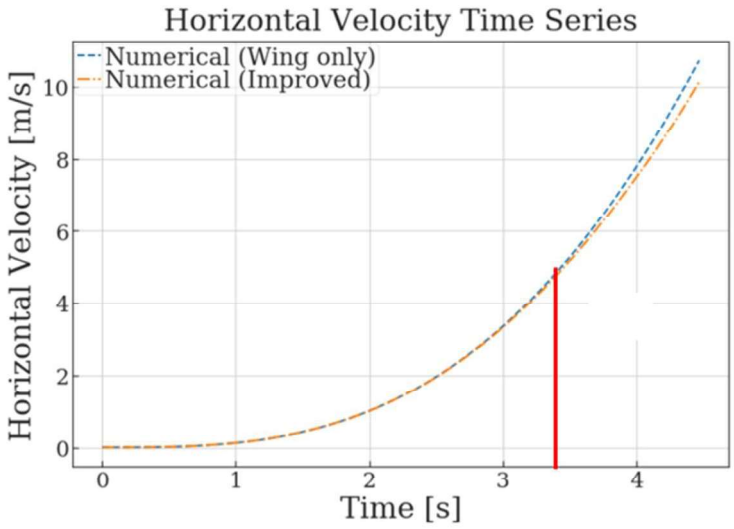

Figure 5.8: The horizontal velocity versus time (simulated, vertical equilibrium point marked)

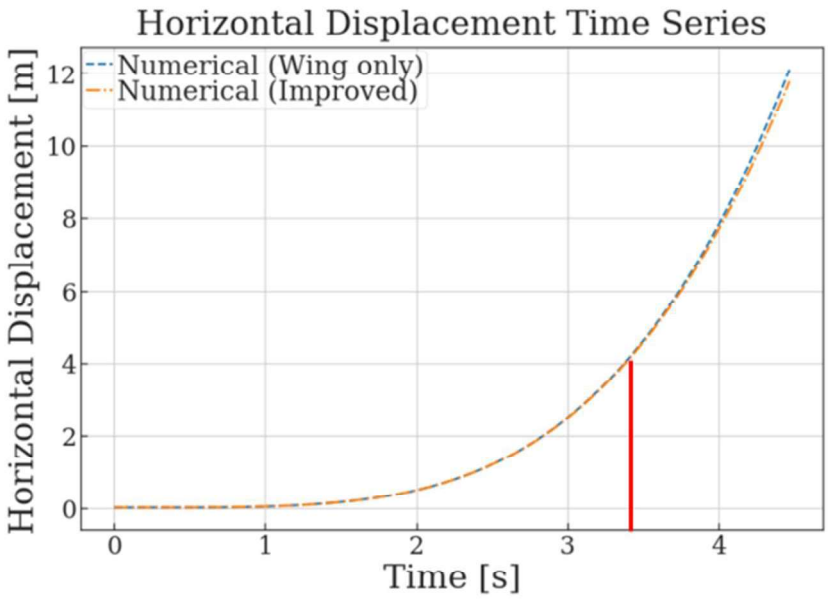

Figure 5.9: The horizontal displacement versus time

(simulated, vertical equilibrium point marked)

The horizontal velocity of 11 m/s indicates at the UAV forward flight speed is relatively high. That brings a warning for the later actual forward transition flight test. The transition flight test should be conducted carefully and safely at the indicated forward flight speed. There is not much difference in horizontal velocity and displacement results using different drag curves as well. As the UAV speeds up, the difference in horizontal velocity starts to appear. The horizontal speed is dominant for drag estimation and the coefficient of the drag for slow speed does not make too much of a difference in comparison to the large thrust provided by the motors. With the predicted horizontal and vertical displacement, the forward transition flight trajectory is plotted in Figure 5.10. Figure 5.10 indicates, the aircraft flies forwards and climbs up during the hover-to-cruise transition with a 0.24% increase in the tail motor thrust. The change in horizontal displacement is greater than the change in vertical displacement. The goal is to have a minimum change in vertical displacement during the transition.

Additionally, a climb-up motion is preferred to the dive-down motion as the dive-down motion might require a higher flight altitude requirement to be able to safely transition.

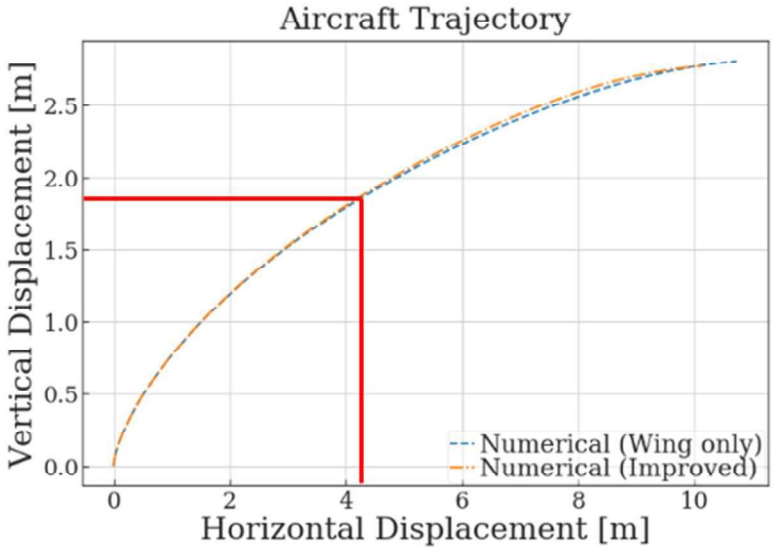

Figure 5.10: The aircraft trajectory for $\Delta T_r = 0.24\%$
(simulated, vertical equilibrium point marked)

Figure 5.11, the ratio of drag to horizontal thrust in the time series is plotted to show the percentage drag force in terms of the horizontal thrust component.

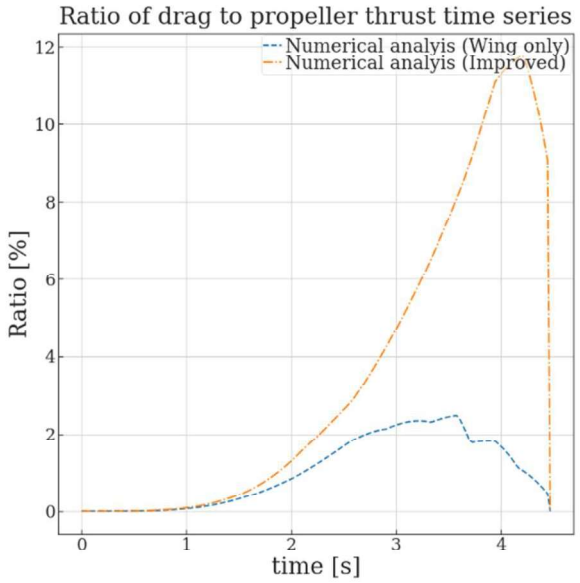

Figure 5.11: The drag-to-thrust ratio versus time (simulated)

Based on Figure 5.11, the overall drag force compared to the propeller horizontal thrust component was one magnitude smaller. This result indicates that there is plenty of potentials to lower the front and tail motor speed during the cruise. As a result of the increased airspeed, the drag increases resulting in a decrease in the thrust-to-drag ratio during the forward transition process. As the airframe continues to tilt, the drag force is reduced as the angle of attack decreases and the flow reattaches. Meanwhile, the horizontal thrust component increases as the airframe tilts down. These combined effects result in a significant drop in the drag-to-thrust ratio after the UAV reaches instantaneous vertical equilibrium. The numerical analysis with different drag curves makes no difference at the beginning of the forward transition as the relative airspeed is small initially. However, the difference in drag-to-thrust ratio starts to appear as the forward transition proceeds. The increase in relative airspeed enlarges the difference in drag estimation.

Figure 5.12 shows a general trend study of the simulated aircraft trajectory for various percent changes in tail motor thrust (ΔT_r). Generally, the higher the percent change of thrust results in sharper dive down. The increase of tail motor thrust initially helps to obtain a higher positive net vertical force. However, the fast airframe tilting transition results in a fast loss of the vertical force component by motors and not enough time to gain airspeed for wing lift. On the other hand, a slow airframe tilting brings other issues and concerns. For example, when the change of tail motor thrust is only 0.1%, the vertical and horizontal displacement is much larger compared to faster airframe tilting results. That results in a large test field needed and a much faster flight speed during the transition. While conducting flight tests, a higher flight speed raises safety concerns as the total kinetic energy increases. This general trend study provides insight into reasonable airframe tilting speed and corresponding UAV flight trajectory.

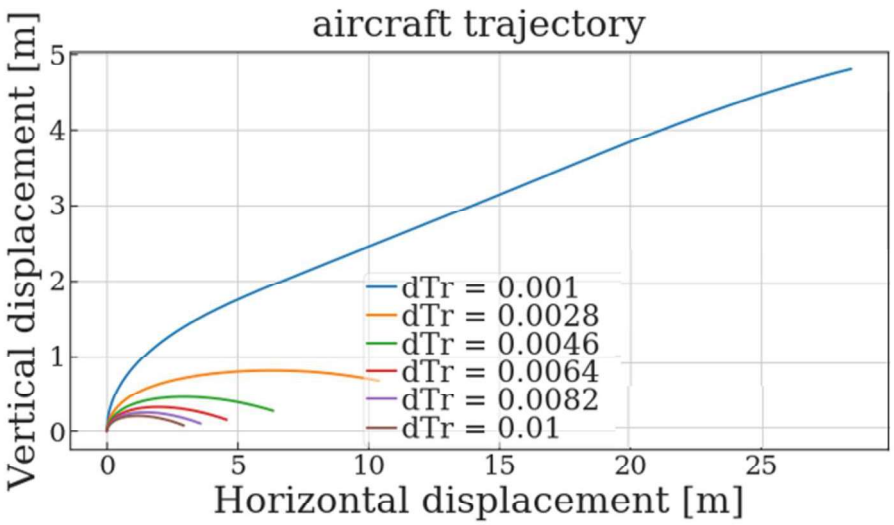

Figure 5.12: The aircraft trajectory for a range of ΔT_r (simulated)

To sum up, based on Figure 5.6, at the transition endpoint, the slope of vertical velocity is zero indicating a net zero vertical acceleration. However, based on figure 5.8, the slope of the horizontal velocity is still positive which means the net horizontal acceleration is non-zero.

The thrust is greater than the drag at the transition endpoint and the aircraft will continue to accelerate. That gives some insights for future horizontal flight mode studies. After the transition mode end, the cruise flight mode might consider using the tail motor to adjust the angle of attack for flight attitude control. Furthermore, when a design cruise speed is reached, the pilot might consider gradually lowering the front and tail motors' thrust to maintain a force equilibrium in the horizontal direction. Due to the decrease in thrust requirement, the tilted-airframe UAV is more power efficient than the traditional tri-copter during the cruise phase.

Chapter 6
Model Validation

6.1 UAV Flight Test

Three main flight tests were completed for the model validation. The indoor flight test was performed at the Center for Spaceflight Research facility (CSFR) at UC Davis. First, the tilted-airframe UAV is tested and tuned using the 5 DOF test rig mentioned previously. The test rig tethers the UAV and thereby allows safe tuning of the UAV flight controller in case of unstable flight behavior. However, the attached test structure weight and applied friction add extra forces to the UAV net forces. These changes in the UAV's net forces during the test flight might result in a slightly different flight behavior from the UAV free flight in the air. Additionally, the UAV has a total of six DOF while the test rig only provides five DOF. Therefore, a tethered flight indoor test was completed after the tilted-airframe UAV was successfully tuned for hover stability. For this test, the UAV was tethered using a metal chain connected to a dumbbell on the ground which restricts the flight radius of the tested UAV. Any uncontrolled flight situation will be limited by the metal chain and people and property will not be at risk. The benefit of the tethered method minimizes the impact on the UAV flight behavior if the chain is not stretched. The tethered method allows all six DOF for UAV motion and the test of UAV dynamic response possible. Figure 6.1 shows the image while the UAV is tethered and hovering.

Figure 6.1: Indoor tethered hovering

Lastly, the outdoor restriction-free flight test was conducted at Woodland-Davis Aeromodelers RC field. The WDA RC field is the model aviation club located between Woodland and Davis, California [22]. The WDA RC field is a designated area that allows the test of UAV flight behavior safely. The UAV hovers freely and fine-tunes at the RC field and prepared for a forward flight transition. The forward flight transition test was conducted only when the wind speed was below 5 knots to minimize the wind impact on the aircraft's motion. When performing the forward flight transition, only the manual pitch command is sent to the UAV flight control as in the flight simulated in Section 5. A small amount of change of tail motor thrust initially and constant motor thrust during the transition is considered. The UAV autonomously controls its yaw and roll moments to counter small wind disturbances meaning that no manual commands of roll and yaw are given during the forward transition to control the variables. The actual flight logs are recorded and proceeded to compare with the numerical modeling results.

6.2 Results Comparison and Discussion

These three forward transition flight test data were recorded. The raw data was processed using the MATLAB flight log analyzer, while the comparison plots were plotted using Python. The solid lines represent the actual flight data obtained from each test trail, with a 0.24% increase in tail motor thrust. While the dashed lines represent the corresponding numerical modeling results. Figure 6.2 compares the tilt angle in the time series.

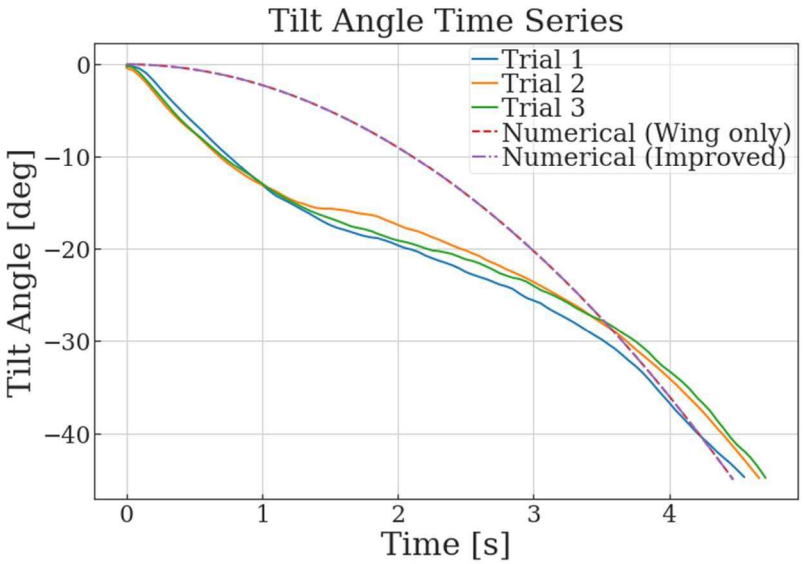

Figure 6.2: Tilt angle versus time (result comparison)

Based on Figure 6.2, the tilt angle has a similar general trend, and the result matches within the acceptable range, especially during the end of airframe tilting. Initially, there is a noticeable difference between the flight log data and the numerical modeling. The numerical modeling assumes the tail motor operates at a constant speed during the transition with instantaneous ΔT_r=0.24% from hovering. While in the actual flight test, the motor needs time for varying the rotation speed and the lag in pitch rate control together causes the initial overshoot of the pitch rate. That is the reason why the UAV airframe tilts down faster at the beginning of the forward transition. As the rate controller matches the simulated pitch rate, the results of the forward transition match at the end.

Figures 6.3 and 6.4 shows the comparison results of the horizontal velocity and displacement. The flight log result shows that the horizontal velocity is higher than the predicted values initially. That follows similar reasoning as tilt angle results. As the UAV tail motor thrust overshot initially, the flight result of the horizontal velocity should be greater than the simulated result. Although the winds were light during the flight tests, small wind gusts and variations in wind speed affected the test results. The same reasoning applied to the horizontal displacement plot.

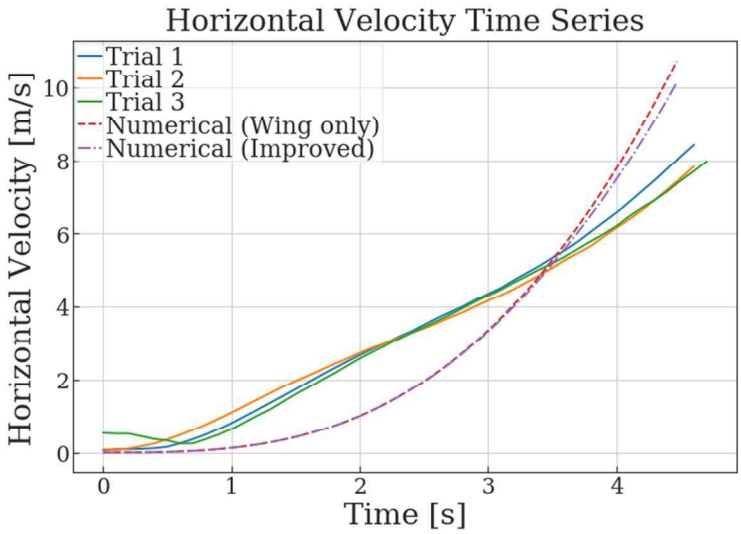

Figure 6.3: Horizontal velocity versus time (result comparison)

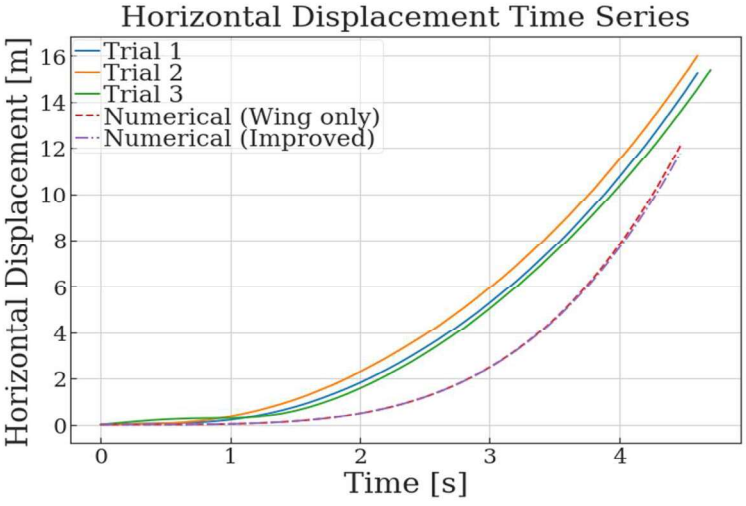

Figure 6.4: Horizontal displacement versus time (result comparison)

Figures 6.5 and 6.6 shows the comparison results of the vertical velocity and displacement. The flight log result shows that the vertical velocity is lower than the predicted values initially. Based on the tilt angle result plot, the flight data indicates a faster-than-expected nose-down tilting. That causes a faster-than-expected loss in the vertical force component. As a result, at the beginning of the transition, the actual vertical velocity would not increase as much as in the simulated case. As the transition proceeds, the actual vertical velocity catches up with the simulated results. Moreover, the significant difference in vertical velocity for the flight test data indicates the wind condition impacts the vertical velocity.

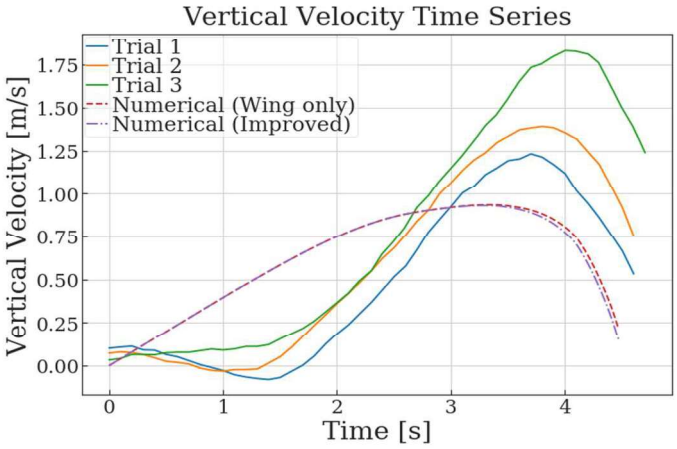

Figure 6.5: Vertical velocity versus time (result comparison)

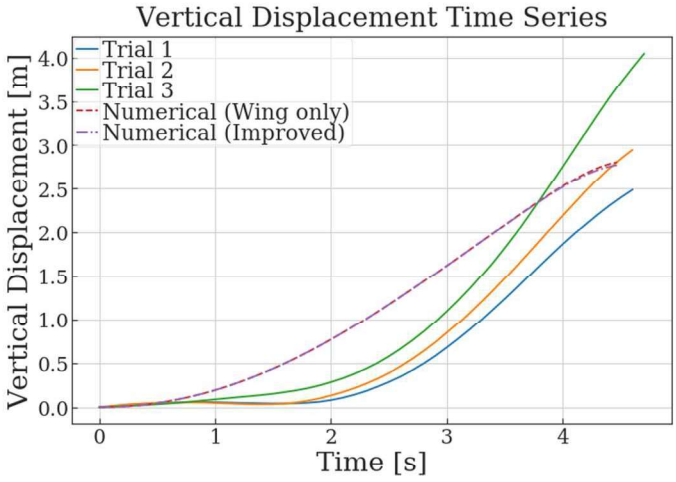

Figure 6.6: Vertical displacement versus time (result comparison)

Figure 6.7 shows the aircraft trajectory of the flight test result and simulated result. The trajectory indicates the UAV climbs up and moves forward during the hover-to-cruise transition. The flight data has higher displacement travel in both vertical and horizontal directions compared with the modeled result. The main factor that causes the difference in the flight result is the tail motor thrust control. As a result of the initial overshoot of the tail motor thrust and the lag in the control algorithm, the airframe tilts rapidly at the beginning, causing the difference. Despite the difference in magnitude between test and numerical analysis results, the numerical model provides useful flight motion prediction and helps determine a reasonable change of tail motor thrust for the actual flight test.

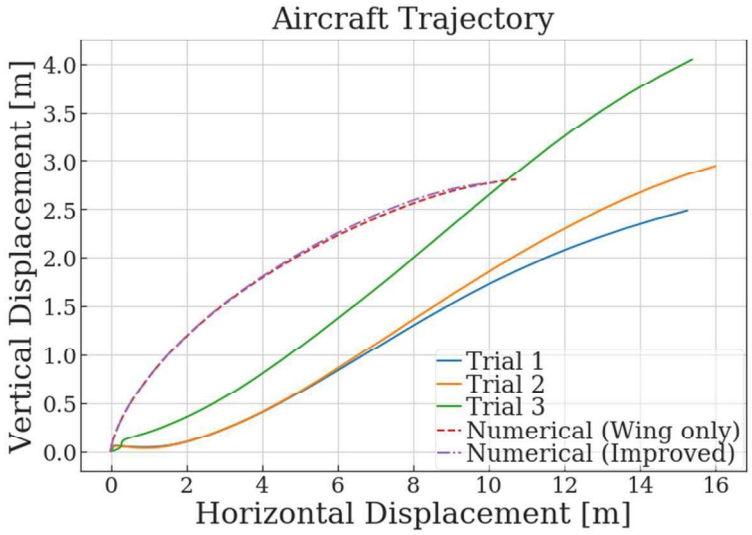

Figure 6.7: Aircraft Trajectory (result comparison)

Chapter 7

Cruise Performance Analysis

7.1 Methodology

A flight performance analysis was conducted using aerodynamic assumptions and the physical characteristics of the UAV from Table 3.2. The cruise performance analysis assumes 5000 mAh out of 7000 mAh battery capacity is used for the cruise. The remaining 2000 mAh battery capacity is reserved for UAV take-off, loitering, and landing. Secondly, in cruise performance analysis, the wind condition is not taken into account. However, a headwind will lower the flight range travel and a tailwind increases the range. The propeller efficiency is dependent on multiple variables such as airspeed, propeller pitch and diameter. A propeller's behavior is quite complex and specific to the propeller. Anishchenko's simplified equation can provide a rough estimate of propeller efficiency using airspeed, propeller pitch, and diameter values [4]:

$$\eta_p = 1 - \frac{V\pi P_{pitch}}{cP_{dia}} \quad \text{(eq 7.1)}$$

η_p	Propeller efficiency
P_{pitch}	Propeller pitch
P_{dia}	Propeller diameter
c	Speed of sound in air
V	Airspeed perpendicular to the propeller disk

When cruising at equilibrium, the total lift is equal to the total weight of the UAV, and the total drag is equal to the propeller thrust component in the horizontal direction.

The equations for equilibrium states are:

$$L = L_{wing} + L_{prop} = W \quad \text{(eq 7.2)}$$

$$D = T_{prop_x} = \frac{1}{2}\rho v^2 S C_D \quad \text{(eq 7.3)}$$

L	Total lift
D	Total drag
L_{wing}	Lift generated by wing
L_{prop}	Lift generated by propeller
T_{prop_x}	Horizontal thrust generated by propeller

A variable β represents the angle between the motor and the freestream airflow as:

$$\beta = \alpha + 45^{\circ} \quad \text{(eq 7.4)}$$

β	Angle between motor and freestream
α	AOA

When cruising at equilibrium conditions, the UAV flies horizontally with its flight path aligned with the horizontal. As a result, the tilt angle is equivalent to the angle of attack. The equation that relates the vertical and horizontal propeller force components is:

$$\tan\beta = \frac{L_{prop}}{T_{prop_x}} = \frac{W - \frac{1}{2}\rho v^2 S C_L}{\frac{1}{2}\rho v^2 S C_D} = \tan(\alpha + 45^{\circ}) \quad \text{(eq 7.5)}$$

Based on equation 7.5, the unknown variables are the UAV cruise speed and trim angle of attack. Therefore, the UAV cruise speed can be solved for a given angle of attack. Additionally, the required propeller thrust can also be calculated. Next, the power required to provide the propeller thrust must be determined. The overall aircraft power required for a given thrust can be calculated based on the thrust requirement for each motor and its corresponding power consumption. Figure 3.7 in the previous section provides individual motor power consumption for the corresponding thrust. On the other hand, a total power requirement is derived by summing up the power requirement for each motor for the corresponding thrust.

The thrust ratio between the main motor and the tail motor was constant because the locations of the motor are fixed and the moment arm is unchanged. Figure 7.1 presents the overall aircraft power requirement versus the thrust.

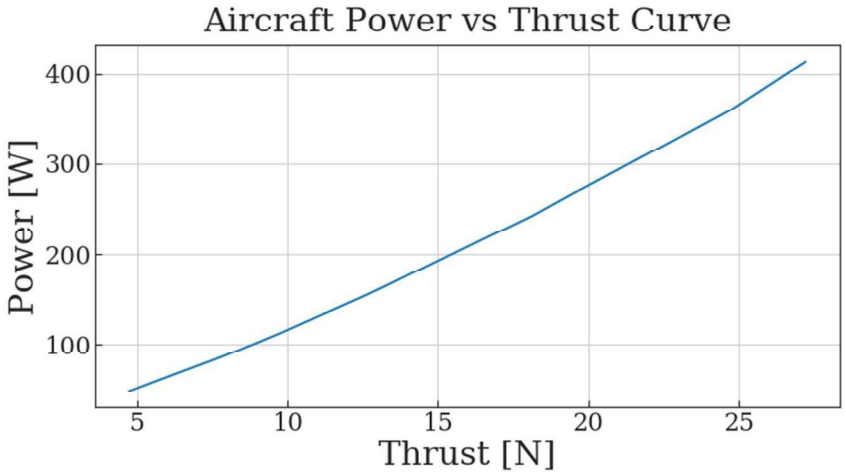

Figure 7.1: UAV power vs thrust curve

The total energy available can be calculated based on the battery capacity, which is the mAh rating, multiply the battery voltage. Then the cruise flight endurance is calculated as:

$$T_c = \frac{E_c}{P_c} \quad \text{(eq 7.6)}$$

T_c Cruise endurance

E_c Energy available (cruise)

P_c Power required when cruising

Lastly, the range is calculated by multiplying the cruise velocity and the cruise endurance. The cruise performance results are included in the following section.

7.2 Result and discussion

7.2.1 Current design cruise performance

Figure 7.2 shows the airspeed required for cruise equilibrium decreases as the angle of attack increases. That is reasonable as lowering the angle during the cruise will lower the coefficient of the lift. The relative airspeed needs to increase for the wing to generate enough lift for cruise equilibrium.

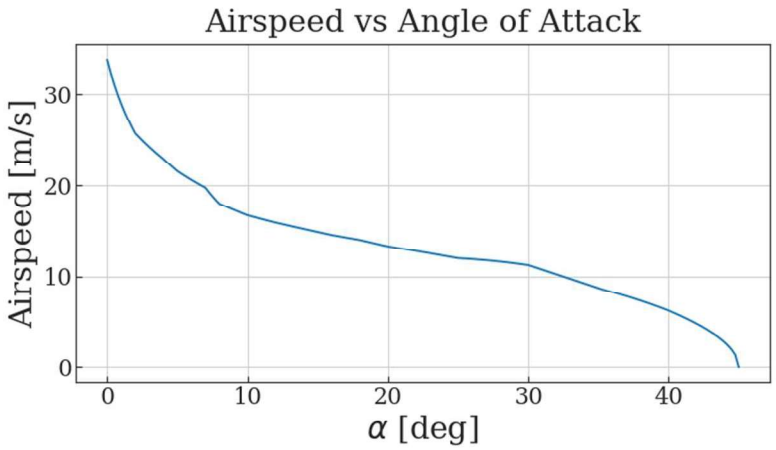

Figure 7.2: Airspeed versus AOA

Figure 7.3 and Figure 7.4 show the thrust required as a function of the angle of attack. The thrust/power required decreases and then increases as the cruising angle of attack increases. The thrust requirement is minimum around the angle of attack of 15 degrees.

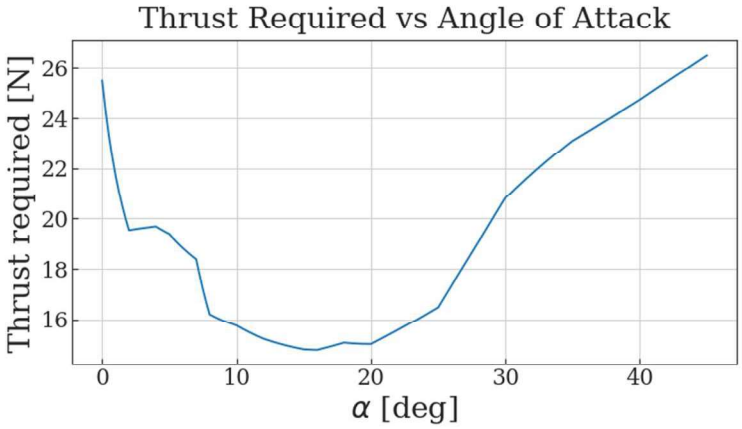

Figure 7.3: Cruise thrust requirement versus AOA

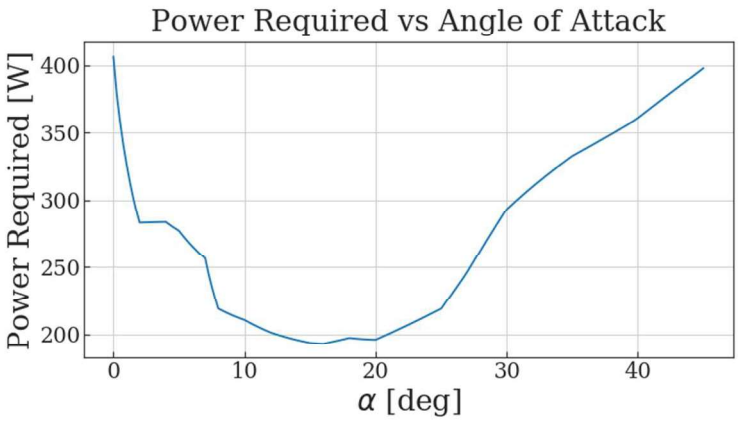

Figure 7.4: Cruise power requirement versus AOA

The ratio of wing lift to the aircraft weight is plotted in Figure 7.5:

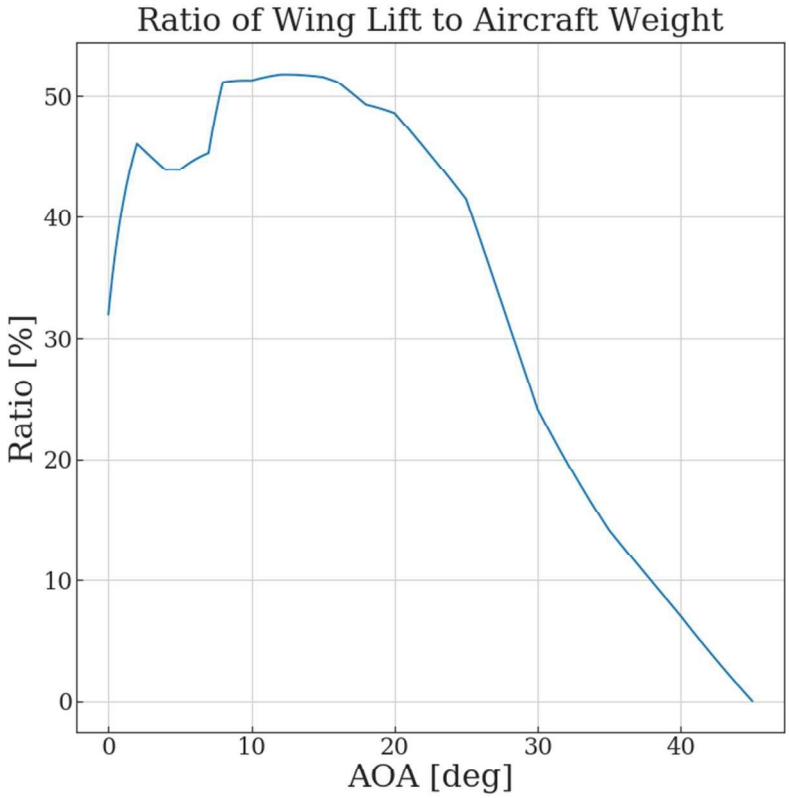

Figure 7.5: Wing lift ratio

Figure 7.5 explains why cruising at 15 degrees angle of attack is the most efficient. The maximum wing lift to aircraft weight ratio is about 52% at 15 degrees cruise AOA.

Figure 7.6 and Figure 7.7 are the flight endurance and range plots. The maximum flight endurance is about 26 mins while the maximum range is 27 km. Professionally-designed multirotor aircraft typically have a flight time between 25 to 30 minutes and a maximum range of less than 10 km [23]. When comparing flight endurance and range, the tilted-airframe UAV has a similar flight endurance but can cover almost triple the flight range. The cruise angles of attack for maximum flight endurance and range are different. The most power-efficient angle of attack will result in maximum flight endurance but not necessarily the maximum range travel. As the range depends on not only the endurance but also the UAV's airspeed. As noted in Anderson's book 'Aircraft Performance and Design', Chapter 8 provides detailed information on parameters to consider when designing a propeller-driven aircraft, including wing loading, lift curve, and thrust-to-weight ratio. The book also offers comprehensive performance analysis for propeller-driven aircraft [24].

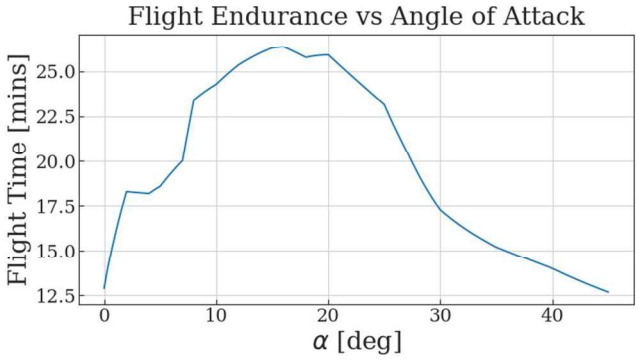

Figure 7.6: Flight duration versus AOA

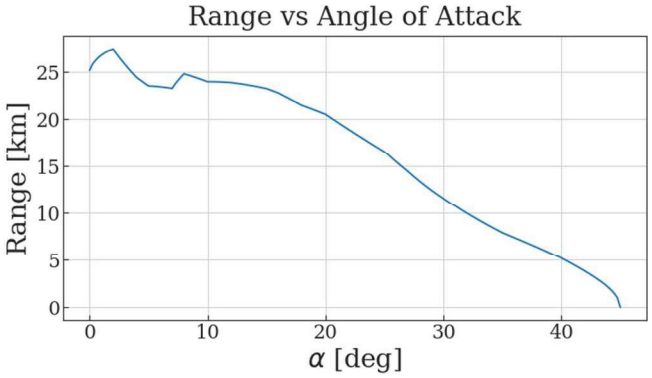

Figure 7.7: Range travel versus AOA

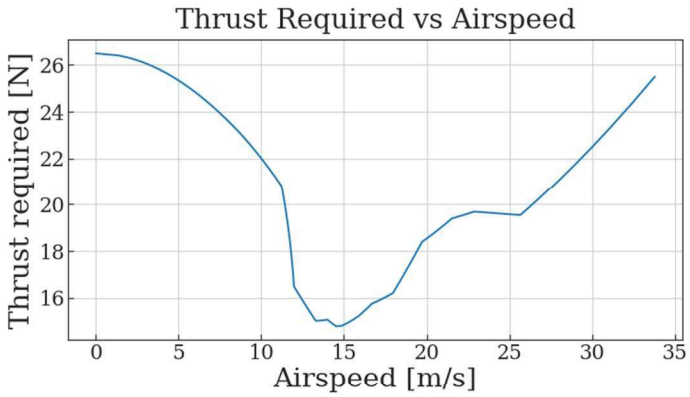

Figure 7.8: Thrust required versus airspeed

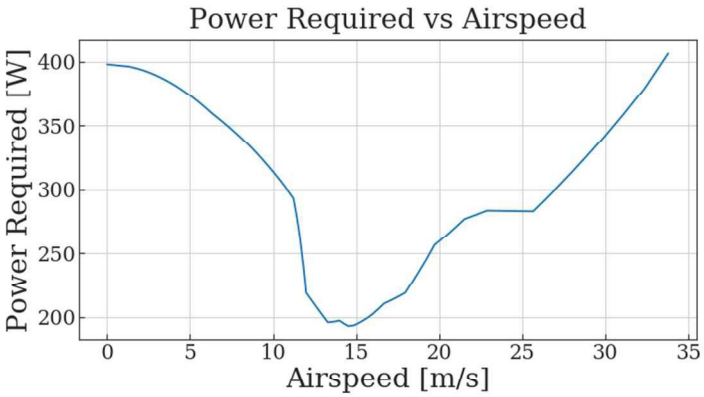

Figure 7.9: Power required versus airspeed

Lastly, Figure 7.8 and Figure 7.9 are the thrust and power required in terms of the cruise airspeed. Figure 7.8 and Figure 7.9 are similar in shape, the difference is more noticeable in the high airspeed (30-35 m/s) region. The tilted-airframe UAV is the most power-efficient when cruising at an airspeed of about 15 m/s. The researcher would like to lower the airspeed for the most power-efficient cruise and further increase the endurance and range travel. One possible solution is to increase the wing area by increasing the wingspan or using a double wing as a biplane aircraft so that the ratio of lift generated by fixed-wing can further increase. Increasing the wingspan improves the aspect ratio for better aerodynamics. However, landing between trees requires limiting the length of the wingspan, and a longer wingspan requires more precise landing control.

A double-winged configuration would not add difficulty to landing precision but would require additional structural weight. A more detailed study is required to determine ways to increase wing area. Section 7.2.2 discusses the effect of doubling the wing area.

7.2.2 Double wing area cruise performance

The doubled wing-size cruise performance is included in this section. One assumption is that doubling the wing-size result in not much change in the UAV's mass (about 4% of the total aircraft weight). In the following double wing area analysis, the added mass of the wing is not counted. Figure 7.10 is the airspeed versus AOA comparison.

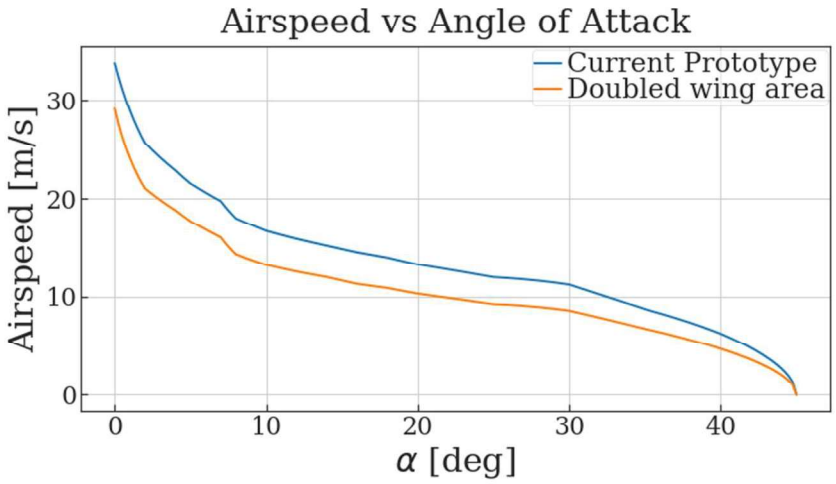

Figure 7.10: Airspeed versus AOA (comparison)

According to Figure 7.10, if the wing area is doubled, the UAV's cruise airspeed decreases for the same cruise AOA. Figure 7.11 and Figure 7.12 shows for the same cruise AOA, the doubled wing area also shows less thrust and power required. Additionally, the UAV cruise is the most power-efficient near 13 degrees AOA.

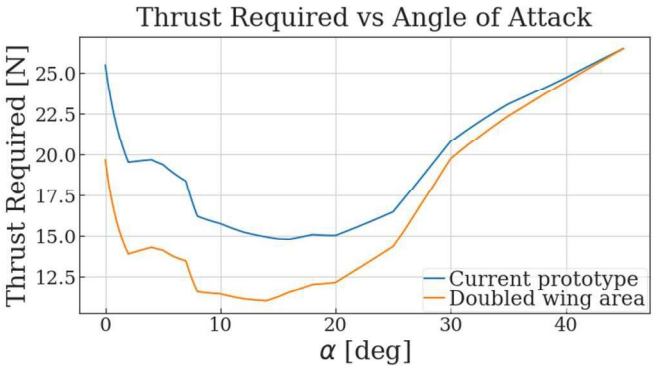

Figure 7.11: Cruise thrust requirement versus AOA (comparison)

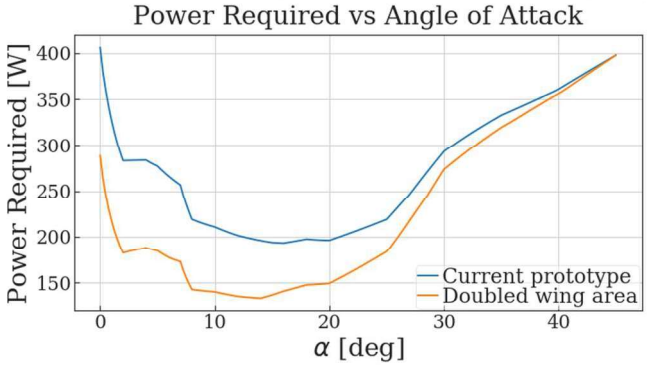

Figure 7.12: Cruise power requirement versus AOA (comparison)

Based on figure 7.13, when cruising at 13 degrees angle of attack, the wing lift ratio is about 65%. The doubled wing area allows more lift generated by the wing which improves the cruise efficiency by increasing the ratio of wing lift to total lift.

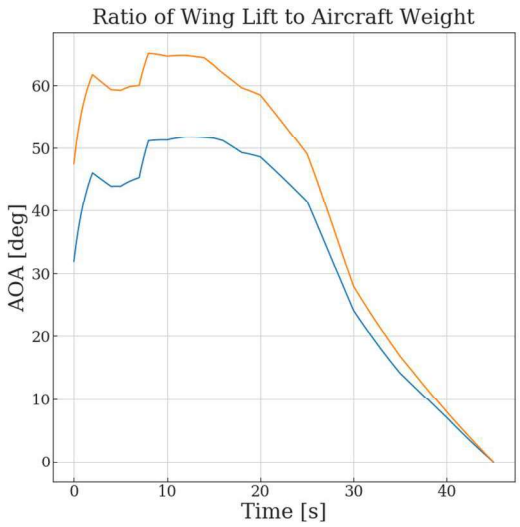

Figure 7.13: Wing lift ratio (comparison)

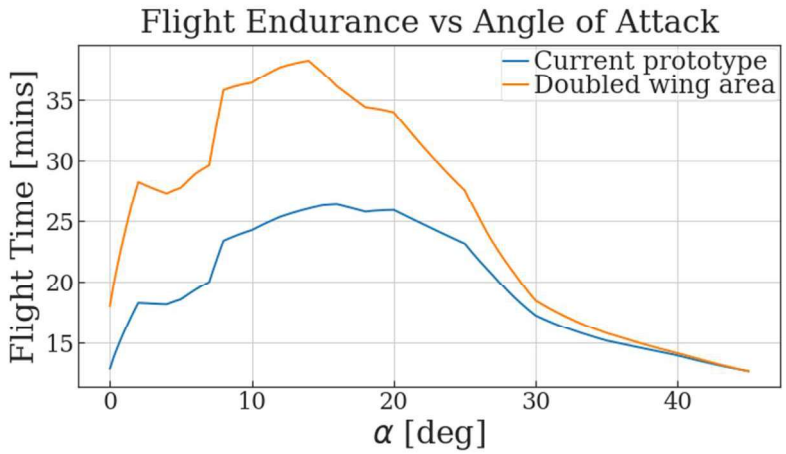

Figure 7.14: Flight duration versus AOA (comparison)

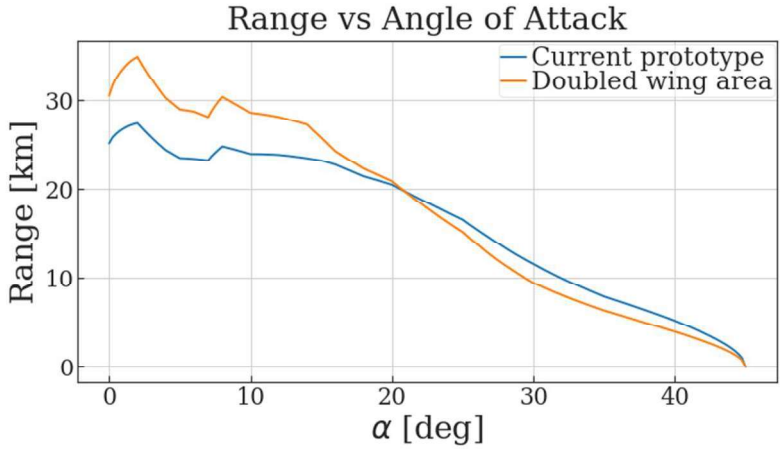

Figure 7.15: Range travel versus AOA (comparison)

Figure 7.14 and Figure 7.15 are the flight endurance and range plots. The doubled-wing area UAV has a maximum flight time of 38 mins while the maximum range is 34 km. If the wing area is doubled, the maximum flight time and range will be greatly improved. The cruise angles of attack for maximum flight endurance and range are different. Based on power consumption, the most power-efficient cruise flight have the longest flight endurance. The range of travel depends on the flight endurance and the cruise speed.

Figure 7.16 and Figure 7.17 are the thrust and power required in terms of the cruise airspeed. The preferred cruise speed (most power-efficient) is about 12 m/s.

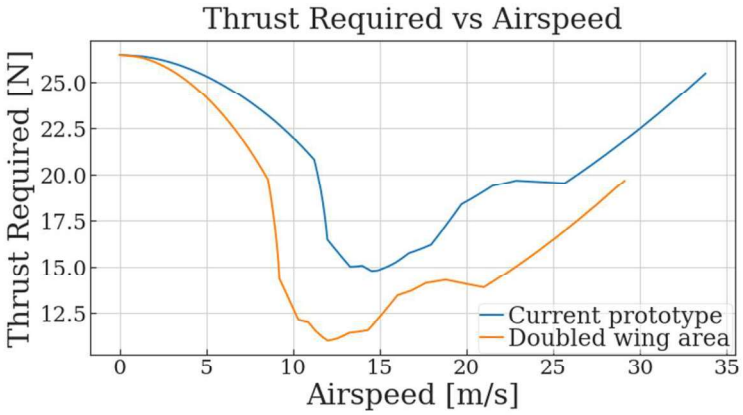

Figure 7.16: Thrust required versus airspeed (comparison)

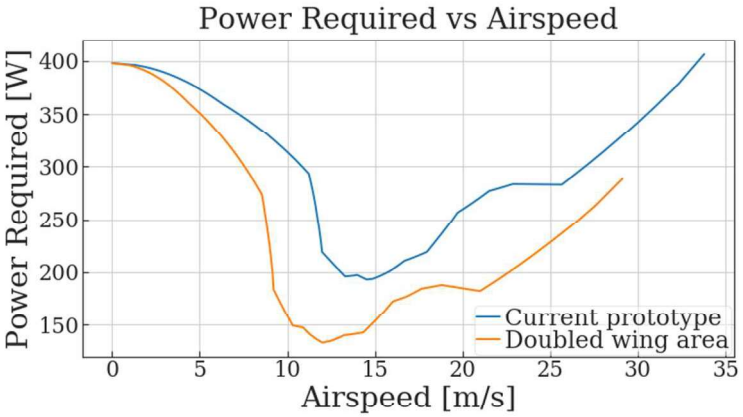

Figure 7.17: Power required versus airspeed (comparison)

Table 7.1 summarizes the cruise performance parameters for the current prototype and the potential doubled wing area prototype.

Table 7.1: Summarized cruise performance table

	Current prototype	Double wing area
Optimum cruise AOA	15 degrees	13 degrees
Optimum cruise speed	15 m/s	12 m/s
Max endurance	26 mins	38 mins
Max wing lift to total lift ratio	52 %	65 %
Max range	27 km	34 km

The results show that doubling the wing area benefits the UAV cruise performance. The UAV therefore can cruise at a lower AOA and speed. Results show both flight endurance and range improved significantly. The maximum flight endurance increased by 45% and the maximum range improved by 26%. To summarize, the cruise performance estimation helps provide the cruise performance characteristic of the current prototype. Additionally, the cruise performance estimation provides insight into further improvements.

Chapter 8
Conclusion and Future Work

8.1 Summary

A research platform using a tilted-airframe UAV was developed for detecting HLB infected citrus trees through air sample collection. The platform was successfully built, modeled, and tested. The test flight demonstrated that the tilted-airframe UAV is capable of vertical takeoff and landing and can conduct a hover-to-cruise (forward) transition flight, as outlined in the mission concept section (Section 2.2.2). The UAV forward transition flight is included in Chapters 5 and 6 which detailed information on transition flight parameters and trajectory information is provided. This research further proved the mission concept originated by Anishchenko [4] not only by using numerical methods to predict the transition flight motion but also by conducting flight tests to verify the simulation. As a result, the general trend of the transition flight parameters from test flight log data agrees with the prediction. However, there are differences between the actual flight behaviors and simulated results. The discussion of the differences is detailed in Chapter 6. There are two main factors to consider for the differences: the airframe pitching rate control and the outdoor flight test environment. The forward transition flight was fully tested and demonstrated but the reverse transition flight was not investigated in this research. At this point, the UAV has not completed the full reverse transition from cruise to hover due to a lack of proper testing facilities to safely test the cruise of the UAV. Despite successfully transitioning the UAV from hover to forward flight, the researcher faced challenges when transitioning back from forward flight to hovering.

The flight test revealed that the process of transitioning from cruise to hover is different from the hover-to-cruise (forward) transition and involves a more significant altitude change.

Additionally, this study updates estimations of tilted-airframe UAV cruise flight performance. The estimated maximum flight endurance is about 26 mins, and the maximum range of travel is about 27 km. The maximum range of a tilted-airframe UAV is outstanding compared to the multirotor which shows the fixed-wing benefits the flight performance during cruise flight. In this way, the tilted-airframe UAV proves its potential for a unique VTOL UAV configuration.

8.2 Future Work

One potential future project is to further study the transition flight of the tilted-airframe UAV. This research simulated and verified the UAV motion for the hover-to-cruise transition but the UAV motion for the cruise-to-hover transition is different. Based on the test flight experience, the beginning of the reverse transition will result in a much higher increase in altitude than the forward transition. As the airframe tilts up, the cruise speed and increases in the angle of attack lead to significant changes in the lift generated by the wing. When transitioning from cruising to hovering, the UAV may experience challenges due to the possibility of flow separation and wing stalling. This can result in a loss of altitude and airspeed, reduce the controllability of the UAV, and lead to a potential loss of control and crash. Further study of the reverse transition flight is necessary to have a full understanding of the mission concept.

Second, the cruise performance estimation in Chapter 7 indicates a potential improvement of the cruise performance by increasing the wing area. Even though, the current test prototype has a distinct flight range travel capability compared to the multirotor, a more detailed study of UAV optimization can help further improve the flight performance of the UAV.

REFERENCES

[1] Ross, K. (2022). California Agricultural Statistics Review. California Department of Food & Agriculture.

[2] Babcock, B. A. (2022). Economic Impact of California's Citrus Industry in 2020. Journal of Citrus Pathology, 9(1). https://doi.org/10.5070/c49156433

[3] CDFA - Citrus - Huanglongbing Pest Profile. (n.d.). Www.cdfa.ca.gov. Retrieved November 22, 2022, from https://www.cdfa.ca.gov/citrus/pests_diseases/hlb/PestProfile.html

[4] Anishchenko, I. (2018). Design, Development, and Validation of a High-Performance Tilt-Frame Unmanned Aerial System for Landing in Tree Orchards [M.S. Thesis].

[5] Palik, M., & Nagy, M. (2019). Brief history of UAV development. Repüléstudományi Közlemények, 31(1), 155–166. https://doi.org/10.32560/rk.2019.1.13

[6] Cornelisse, Diana G. Splendid Vision, Unswerving Purpose. (2002). Department of the Air Force. Wright-Patterson Air Force Base, Ohio: U.S. Air Force Publications, ISBN 0-16-067599-5.

[7] Darling, D. (n.d.). Kettering Bug. Www.daviddarling.info. Retrieved November 13, 2022, from https://www.daviddarling.info/encyclopedia/K/Kettering_Bug.html

[8] O'Malley, D. (n.d.). THE MOTHER OF ALL DRONES. Vintage Wings of Canada. Retrieved Mar 11, 2022, from https://www.vintagewings.ca/stories/mother-of-all-drones

[9] Tsouros, D. C., Bibi, S., & Sarigiannidis, P. G. (2019). A Review on UAV-Based Applications for Precision Agriculture. Information, 10(11), 349. https://doi.org/10.3390/info10110349

[10] Osco, L. P., Marcato Junior, J., Marques Ramos, A. P., de Castro Jorge, L. A., Fatholahi, S. N., de Andrade Silva, J., Matsubara, E. T., Pistori, H., Gonçalves, W. N., & Li, J. (2021). A review on deep learning in UAV remote sensing. International Journal of Applied Earth Observation and Geoinformation, 102, 102456. https://doi.org/10.1016/j.jag.2021.102456

[11] Zappa, C. J., Brown, S. M., Laxague, N. J. M., Dhakal, T., Harris, R. A., Farber, A. M., & Subramaniam, A. (2020). Using Ship-Deployed High-Endurance Unmanned Aerial Vehicles for the Study of Ocean Surface and Atmospheric Boundary Layer Processes. Frontiers in Marine Science, 6. https://doi.org/10.3389/fmars.2019.00777

[12] Zhang, H., Wang, L., Tian, T., & Yin, J. (2021). A Review of Unmanned Aerial Vehicle Low-Altitude Remote Sensing (UAV-LARS) Use in Agricultural Monitoring in China. Remote Sensing, 13(6), 1221. https://doi.org/10.3390/rs13061221

[13] Zou, J.-T., Su, K.-L., & Tso, H. (2012). The modeling and implementation of tri-rotor flying robot. Artificial Life and Robotics, 17(1), 86–91. https://doi.org/10.1007/s10015-012-0028-2

[14] Ali, S., & Gueaieb, W. (2010). Intelligent Flight Control of an Autonomous Quadrotor. Motion Control. https://doi.org/10.5772/6968

[15] Boon, M. A., Drijfhout, A. P., & Tesfamichael, S. (2017). Comparison of a Fixed-wing and Multi-rotor UAV for Environmental Mapping Applications: A Case Study. ISPRS - International Archives of the Photogrammetry, Remote Sensing and Spatial Information Sciences, XLII-2/W6, 47–54. https://doi.org/10.5194/isprs-archives-xlii-2-w6-47-2017

[16] Thamm, F.-P. ., Brieger, N., Neitzke, K.-P. ., Meyer, M., Jansen, R., & Mönninghof, M. (2015). Songbird – An Innovative UAS Combining the Advantages of Fixed Wing and Multirotor UAS. ISPRS - International Archives of the Photogrammetry, Remote Sensing and Spatial Information Sciences, XL-1/W4, 345–349. https://doi.org/10.5194/isprsarchives-xl-1-w4-345-2015

[17] Drew, J. (2016, January 21). New search for VTOL UAVs may resurrect Bell tiltrotor. Flight Global. https://www.flightglobal.com/new-search-for-vtol-uavs-may-resurrect-bell-tiltrotor/119404.article

[18] JOUAV UAS: Drones, Payloads and Software. (n.d.). JOUAV. Retrieved March 15, 2023, from https://www.jouav.com/products

[19] XFOIL Subsonic Airfoil Development System. (2013). Mit.edu. https://web.mit.edu/drela/Public/web/xfoil/

[20] Ostowari, C., & Naik, D. (1985). Post-Stall Wind Tunnel Data for NACA 44XX Series Airfoil Sections. Solar Energy Research Institute.Contract No. DE-AC02-83CH10093

[21] Mixing and Actuators | PX4 User Guide. (n.d.). Docs.px4.Io. Retrieved November 15, 2022, from https://docs.px4.io/v1.12/en/concept/mixing.html

[22] Rc Field | Woodland/davis Aeromodelers. (n.d.). WDARC. Retrieved October 15, 2022, from https://www.wdarc.org

[23] Karanja, A. P. (2022, February 14). Best Long-Range Drones. Droneblog. https://www.droneblog.com/best-long-range-drones

[24] Anderson, J. D. (2012). Aircraft Performance and Design. Boston, Mass. Mcgraw-Hill Higher Education.